Escaping from the Galactic Labyrinths through stellar Daedalus or following AGN Ariadne's wire like Theseus ?

Andrea Grazian (INAF-OAPd)

Escape of Lyman radiation from galactic labyrinths

OAC, Kolymbari, Crete - April 21, 2023

Reionization: What ?

Hydrogen Reionization: major phase transition of the Universe

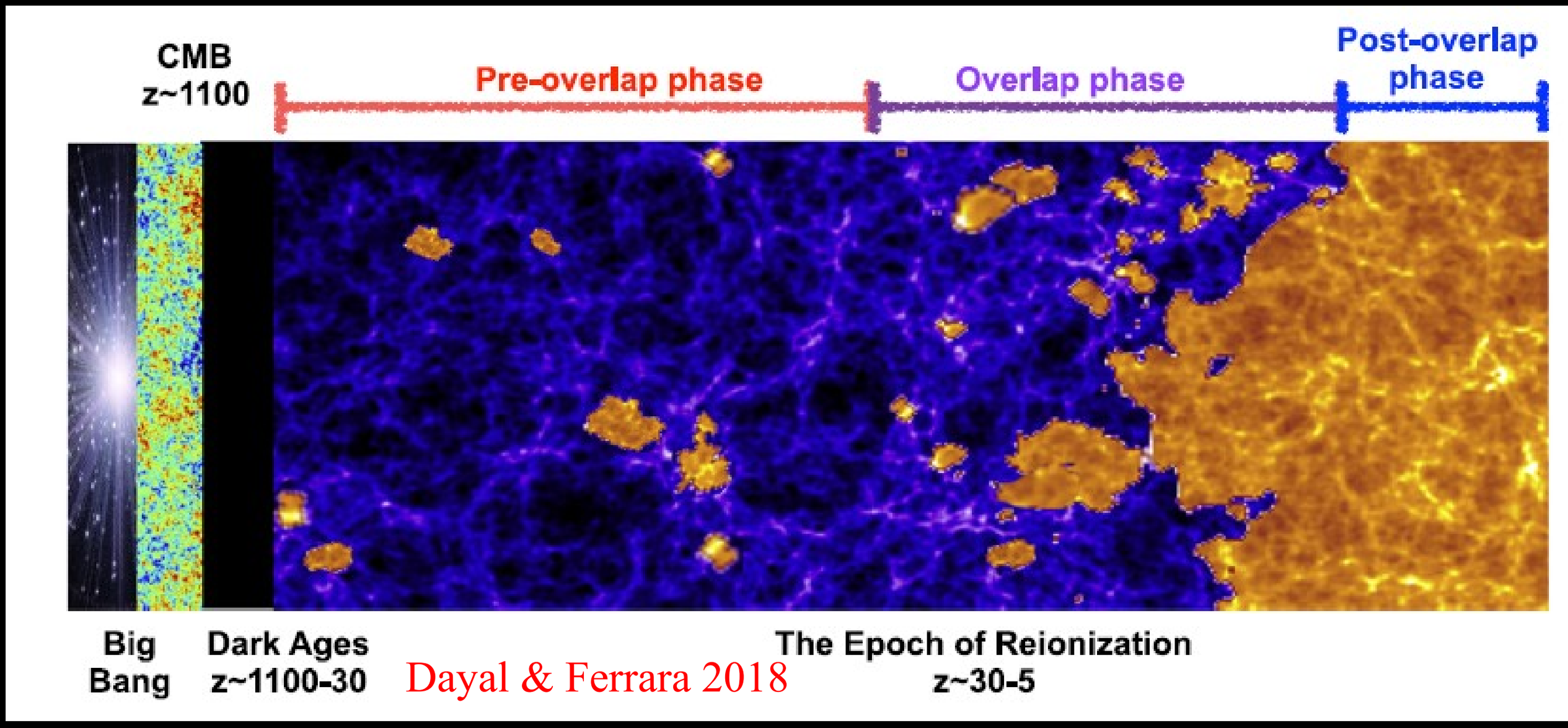

Hydrogen reionization
End of Dark Ages

Epoch of Reionization: When ?

Gunn-Peterson troughs suggest reionization ending at z=5.2-6.0
Ultra Late Reionization
(Fan et al. 2006; Keating et al. 2020; Becker et al. 2021; Bosman et al. 2021; Zhu et al. 2022; Gaikwad et al. 2023)

Planck 2020 result: τ=0.0506+/-0.0086
z_reion~7.0 Delta_z<1.1-2.8
Rapid process
(Akrami et al. 2020; Reichardt et al. 2021)

Gunn-Peterson effect

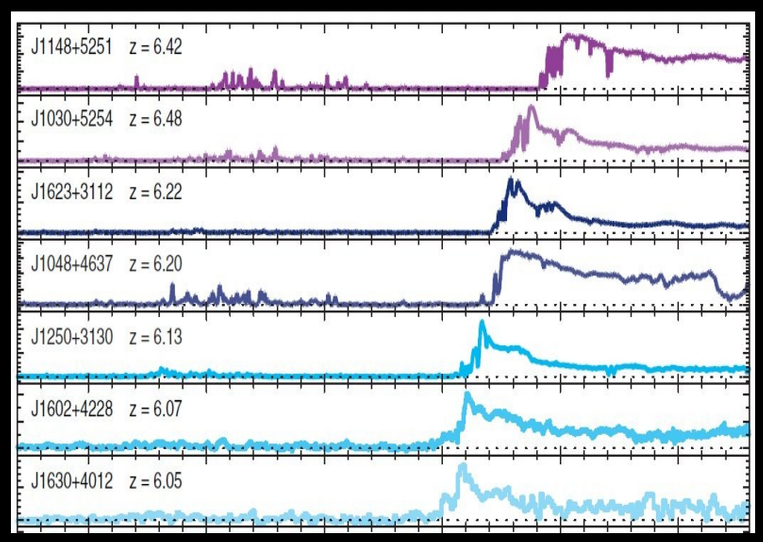

z_reion>5.2

+

Thomson scattering optical depth measured in CMB

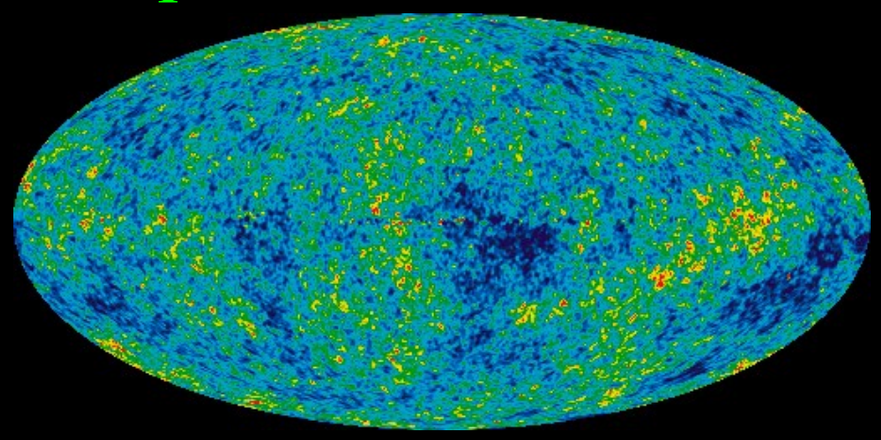

z_reion<8.0

=> 5.2 < z < 8.0

Fast and Ultra-Late Reionization

Production of ionizing radiation

$$\dot{N}_{\rm ion} = f_{\rm esc}\,\xi_{\rm ion}\,\rho_{\rm UV}$$

Ionization rate

$$\rho_{UV} = \int_{L_{min}}^{L_{max}} \phi(L) L dL$$

UV Luminosity Density at
1450 Angstrom rest frame

ξ_{ion}

LyC photons per unit UV Luminosity;
L1450/L900 ratio.

f_{esc}

Escape fraction of LyC photons

Critical paramater: uncertain

How to escape from the Galactic Labyrinths ?

Orthodox or heretic ?

Daedalus and Icarus

Orthodox

Flying easily like
Daedalus and Icarus
close to the stellar
radiation with
the risk of a big fallout ?

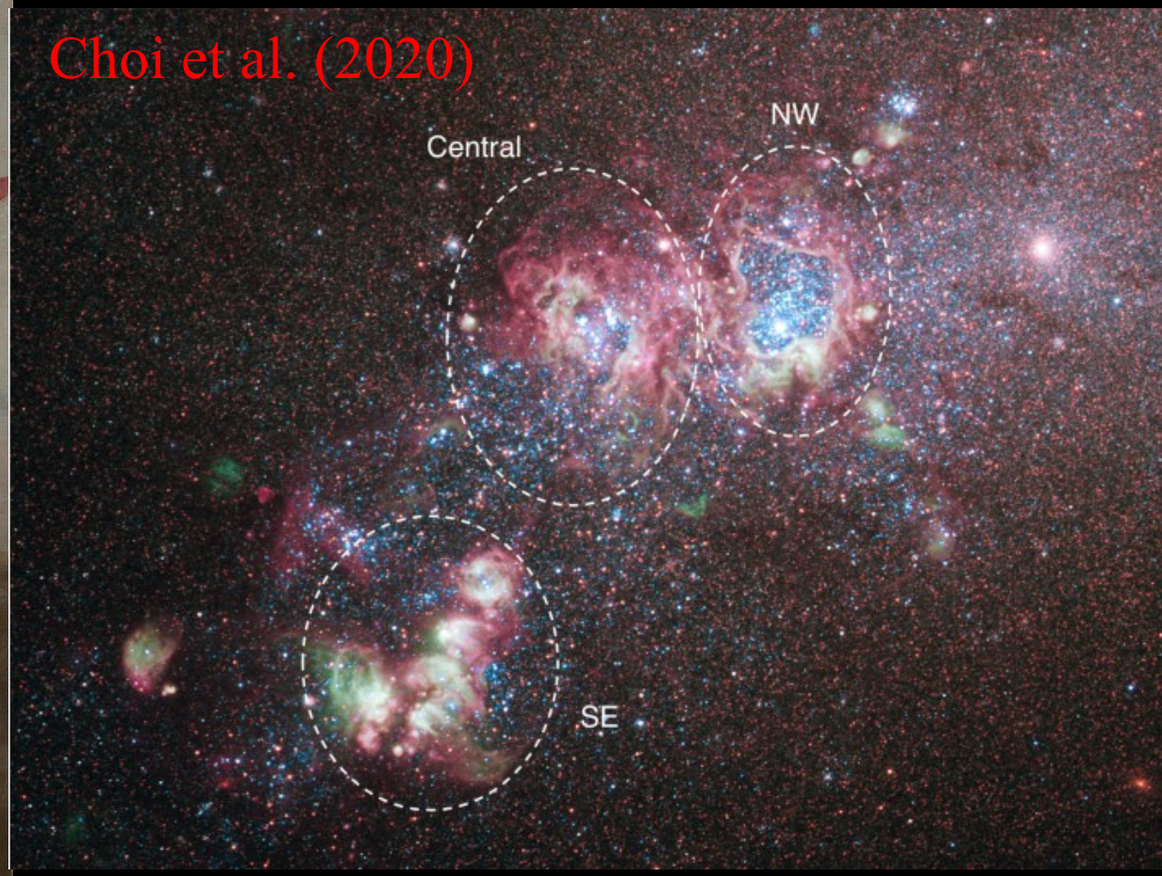

Theseus and Ariadne's wire

Following AGN Ariadne's wire like Theseus, and escaping from the Monster heart towards ionizing freedom ?

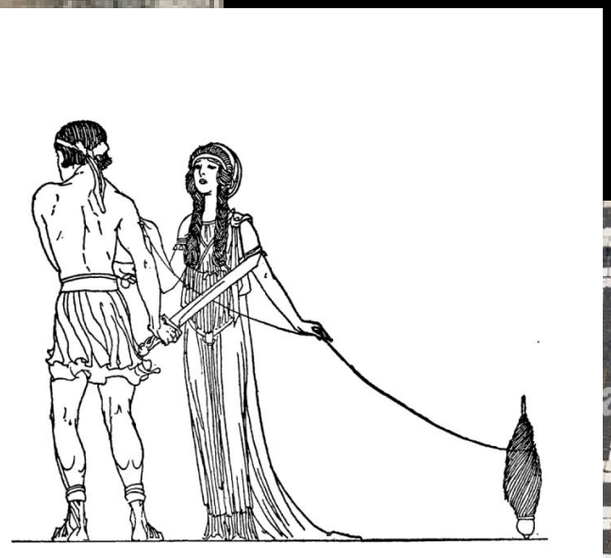

Heretic

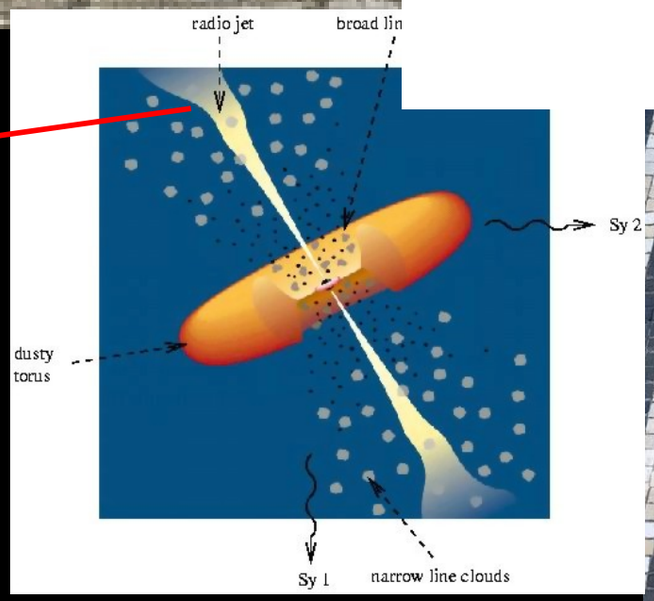

Ariadne's wire

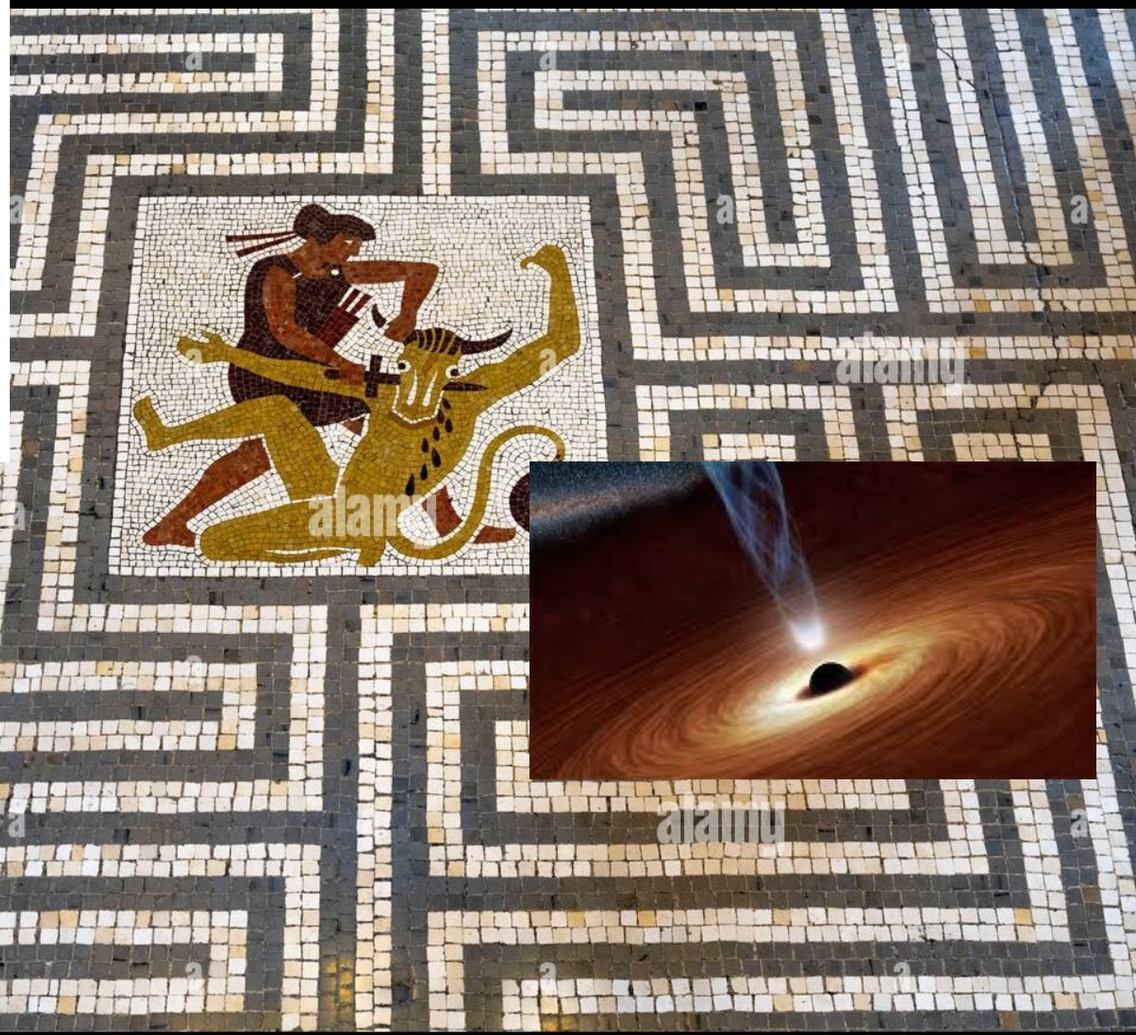

LyC fesc of AGN: imaging

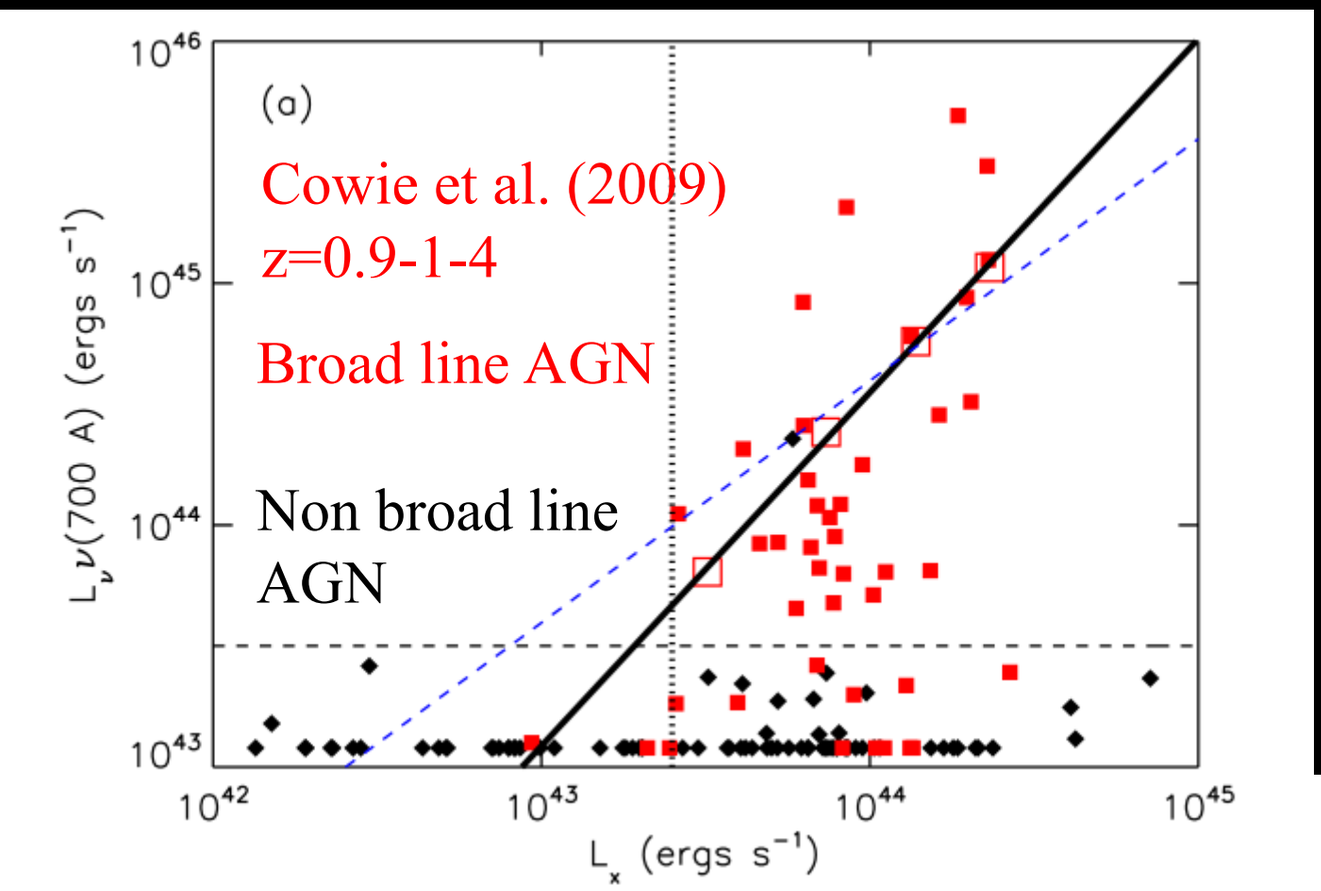

Broad line AGN at z~1 show significant LyC escape fraction (~100%)

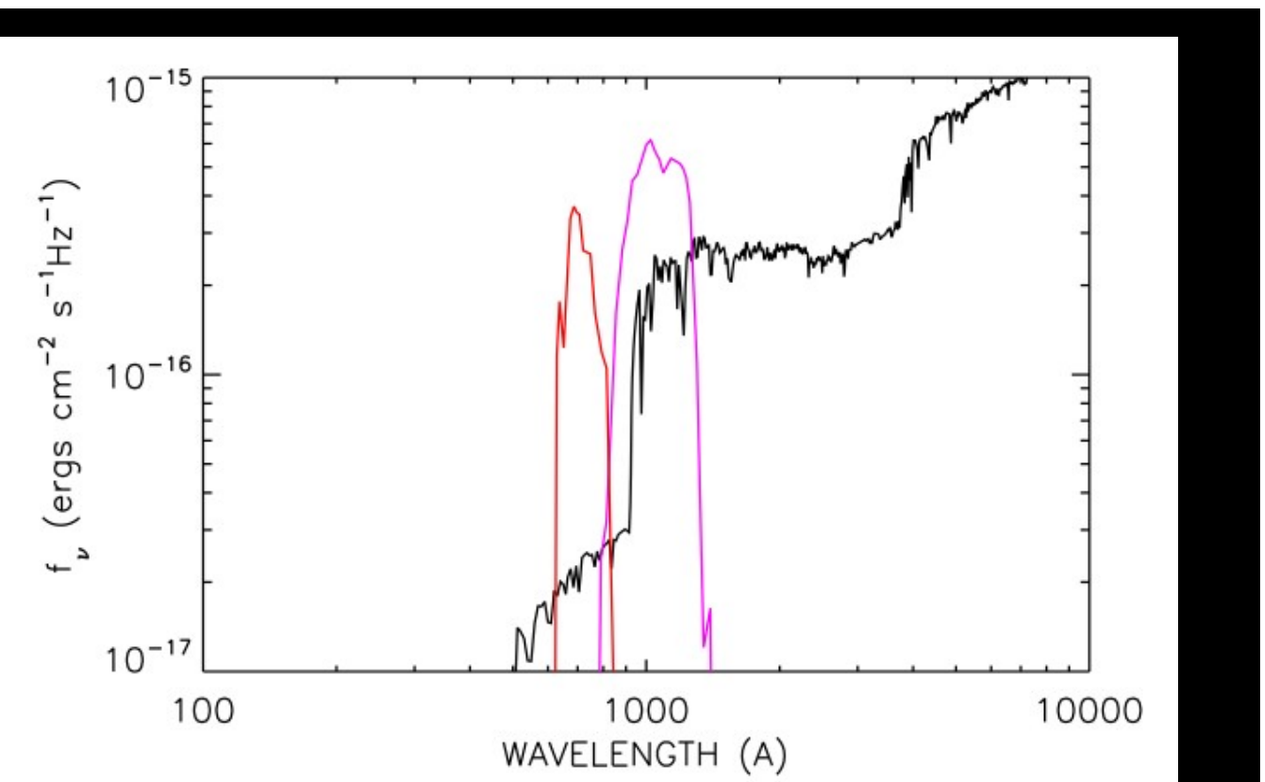

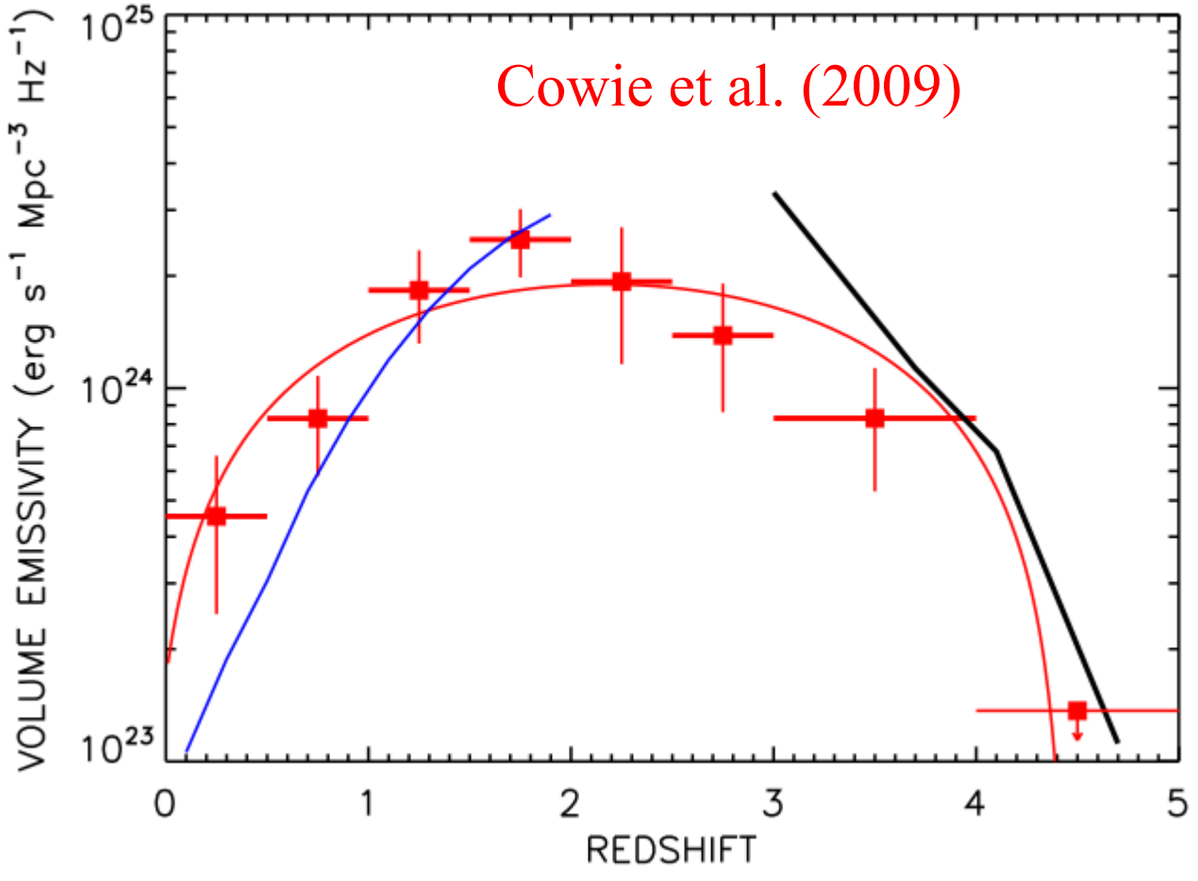

F275W F435W+F606W+F160W

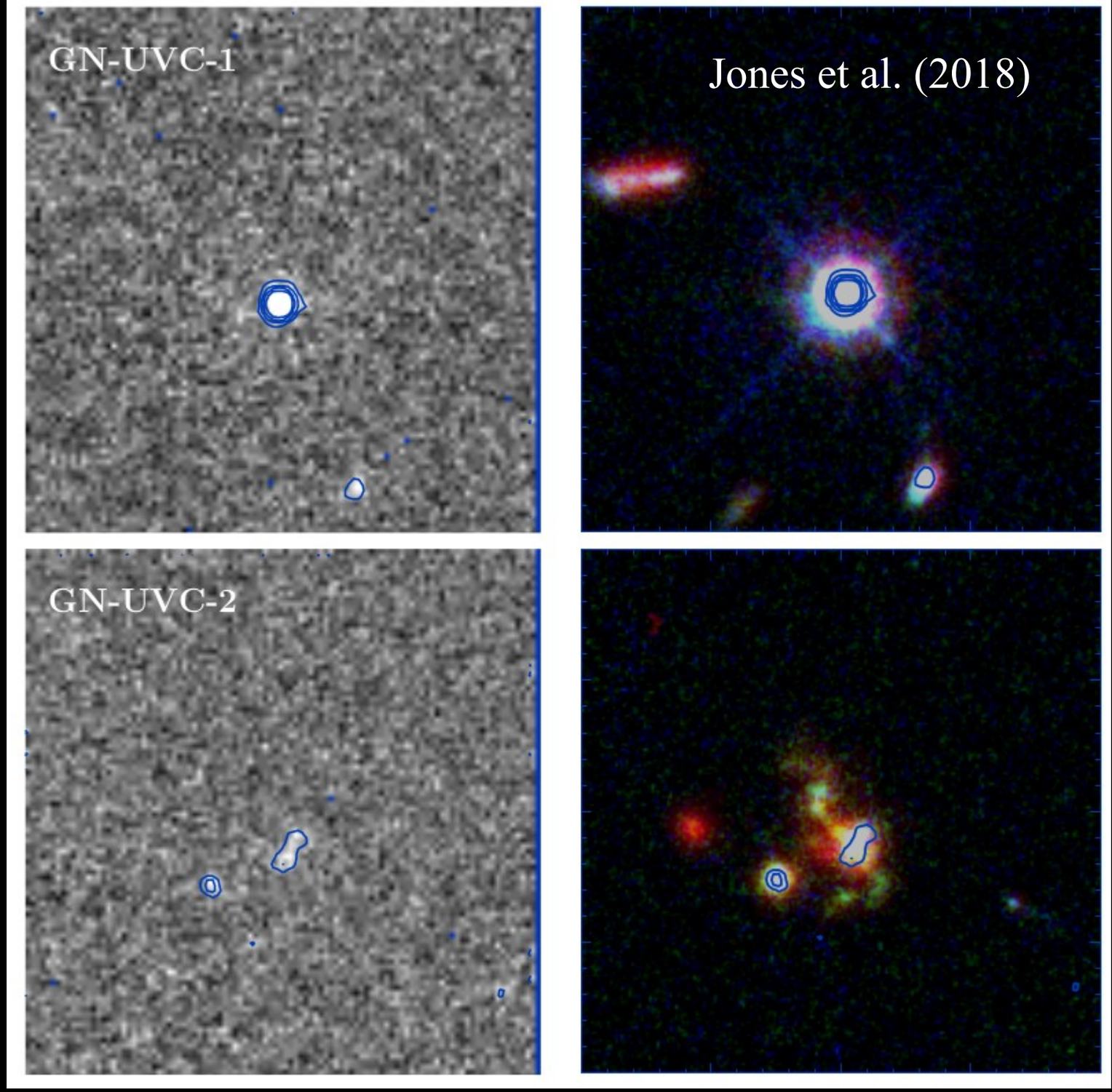

AGN

SFG

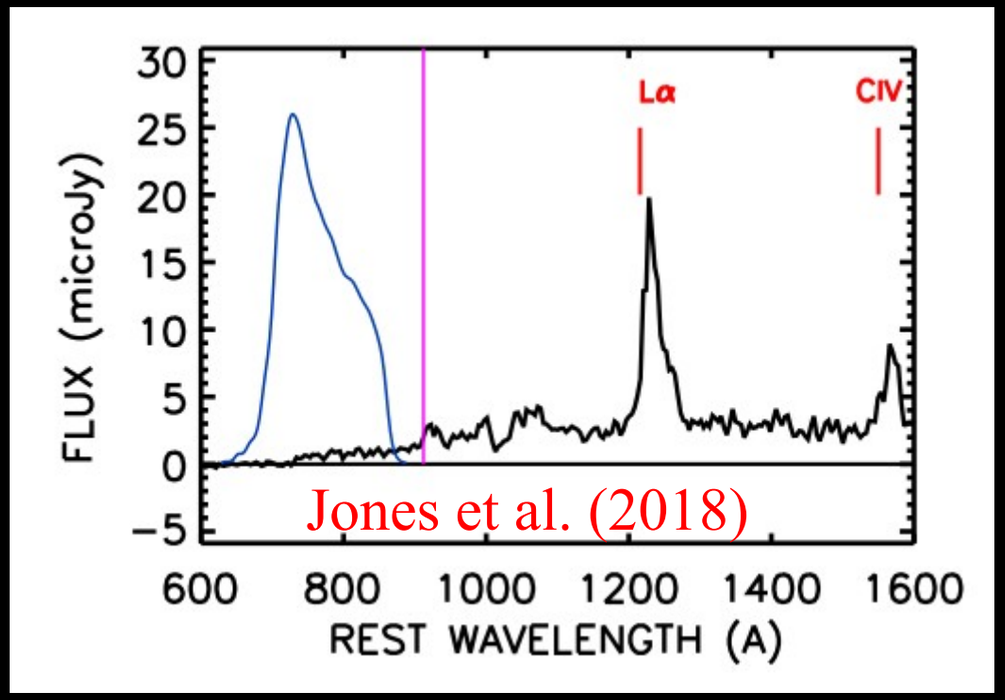

AGN

SFG

All the SFGs detected in LyC at z~2-3 by Jones et al. (2018) show contamination by low-z interlopers. The only confirmed LyC detection is from an AGN at z=2.5.

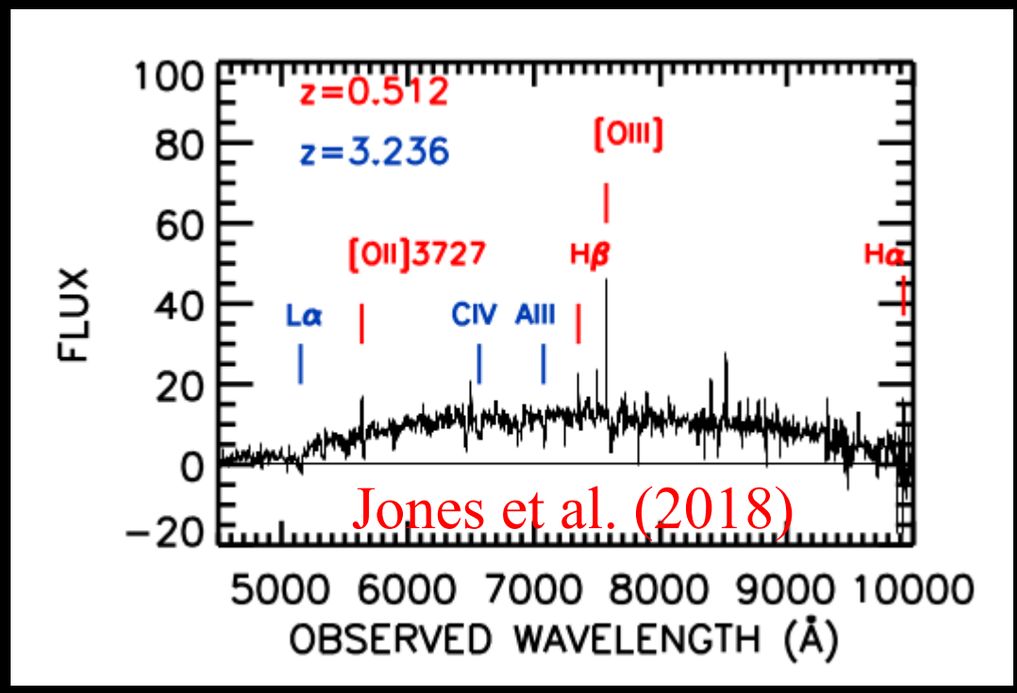

AGNs dominate the ionizing emissivity at z~3. Negligible Contribution by SFGs.

AGN

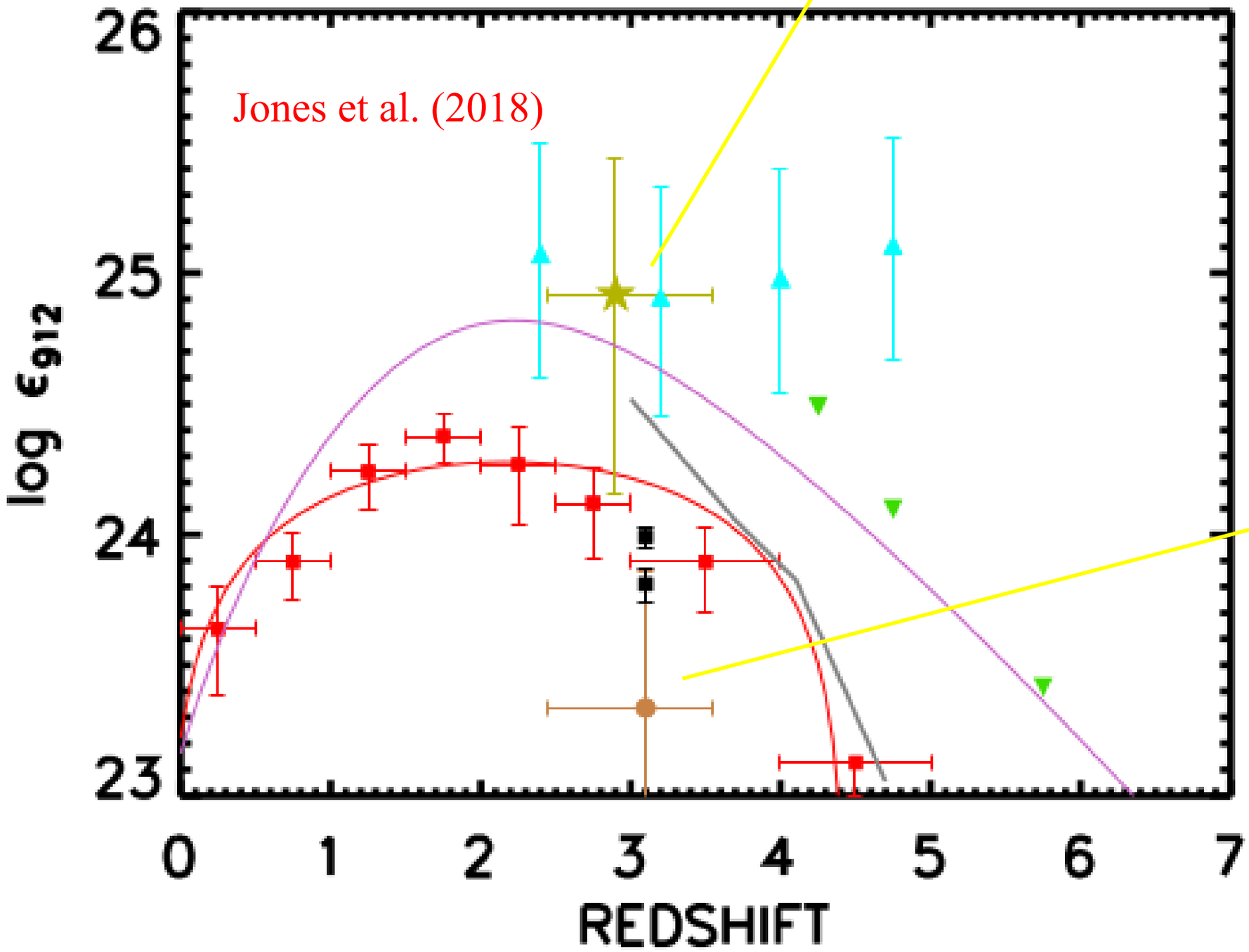

SFG

LyC fesc of faint AGN

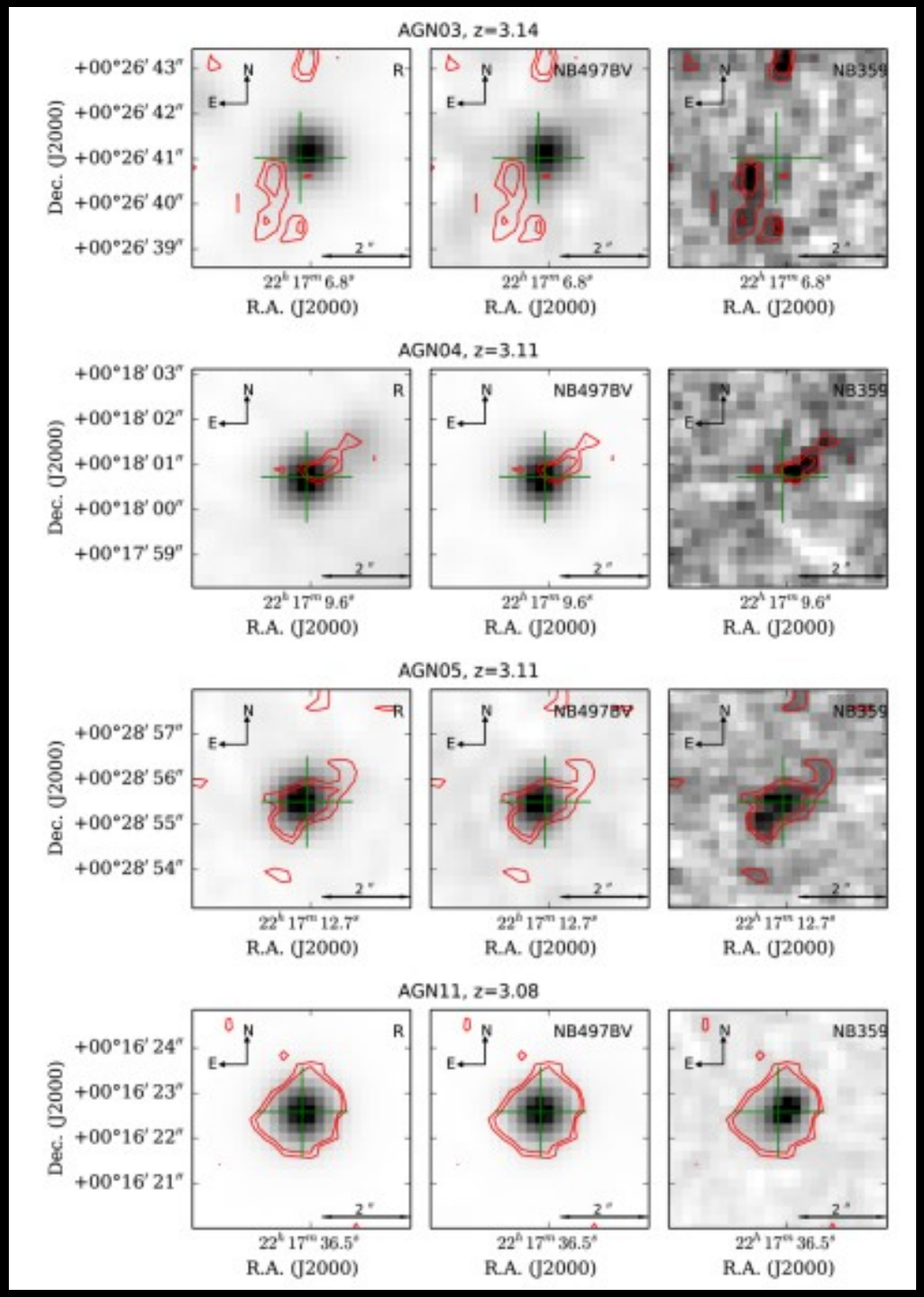

Low escape fraction of faint z>3 AGN ?

Fesc~25%

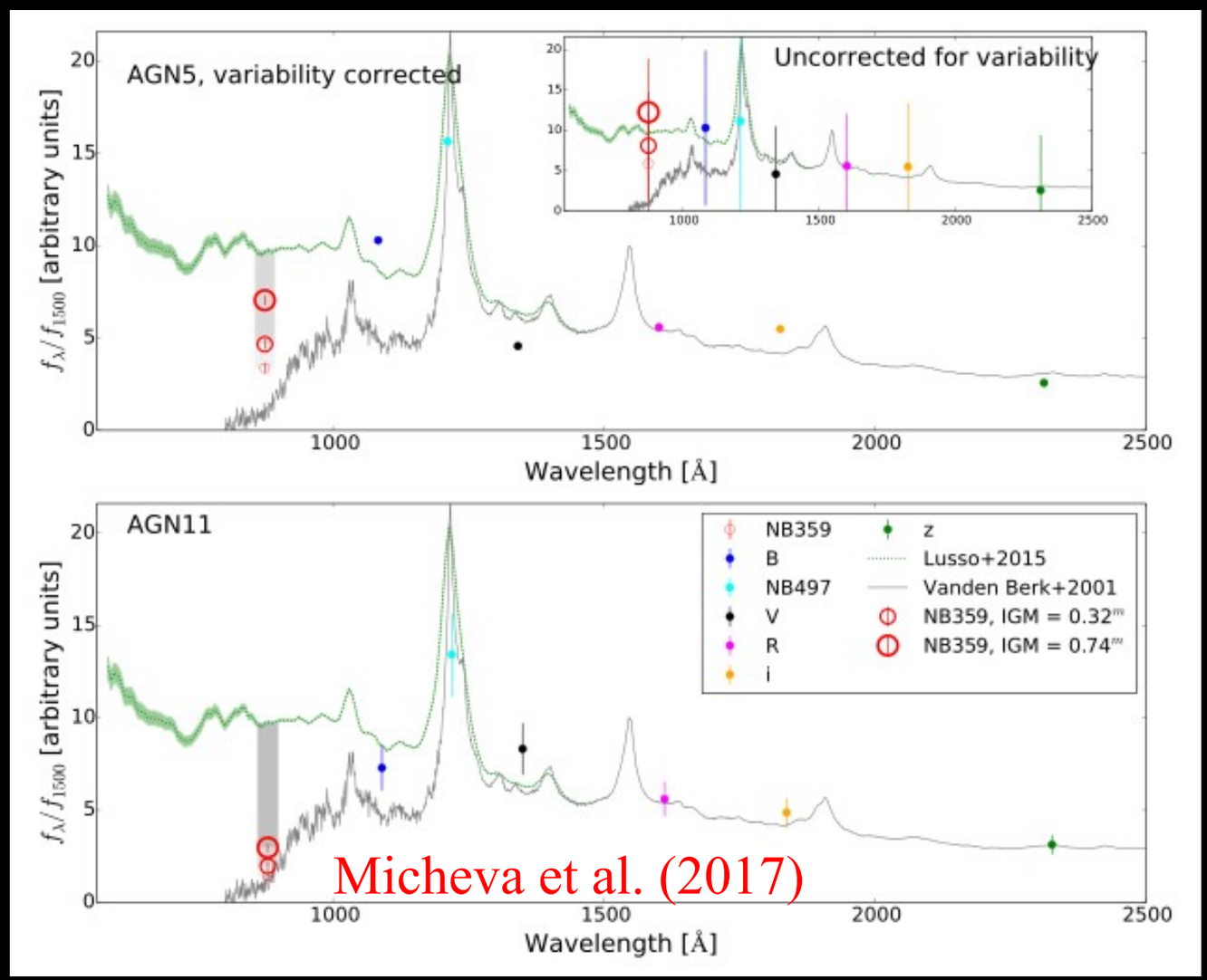

Micheva et al. (2017)

ID	FWHM	R	R(1.2 arcsec)	$NB359$	$NB359$(1.2 arcsec)	$(f_{1500}/f_{900})_{obs}$	$B-V$	$NB359-R$	β (UV slope)	δr
AGN1	0.8	21.83	22.57				1.53		-1.46	
AGN2	0.8	24.75	25.52				0.69		-0.16	
AGN3	0.9	23.78	24.58	26.04 ± 0.20	28.11 ± 0.20	7.97 ± 1.42	1.18	2.25 ± 0.20	-2.47	0.8
AGN4	0.9	24.19	25.00	26.14	27.00 ± 0.12	6.06 ± 0.49	1.01	1.96	-2.41	0.5
AGN5	0.9	23.83	24.62	24.98	26.29	2.88 ± 0.19	-0.46	1.15	0.42	0.2
AGN6	0.9	24.22	25.03				0.73		-2.18	
AGN7	0.8	22.70	23.44				-0.18		-3.13	
AGN8	0.8	21.04	21.80				1.62		-2.34	
AGN9	0.9	25.91	26.79						0.76 ± 0.35	
AGN10	0.9	25.47	26.27				1.45		0.42 ± 0.17	
AGN11	0.8	21.42	22.16	24.09	24.96	11.72 ± 0.27	0.56	2.67	-1.94	0.1
AGN12	1.4	25.09	26.46				1.12		-2.39 ± 0.32	
AGN13	0.8	22.69	23.40				1.02		-0.60	
AGN14	1.2	24.53	25.69				0.87		-0.33 ± 0.18	

Micheva et al. (2017)

ID	λ_{eff}^{LyC} (Å)	$f_{esc}^{\tau=0}$	$f_{esc}^{\tau=0.32}$	$f_{esc}^{\tau=0.74}$	err(f_{esc})
AGN3	867.1	<0.008	<0.011	<0.016	
AGN5	873.5	0.35	0.48	0.73	0.30
AGN7	873.9	<0.003	<0.004	<0.007	
AGN11	879.0	0.15	0.20	0.31	0.27

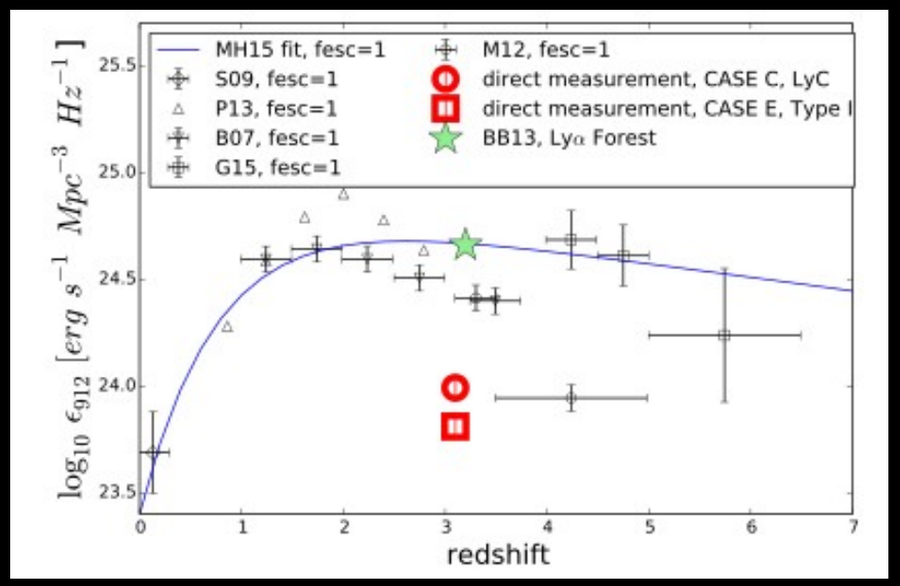

The contribution of AGNs to ionizing emissivity is 3-5 times lower than required.

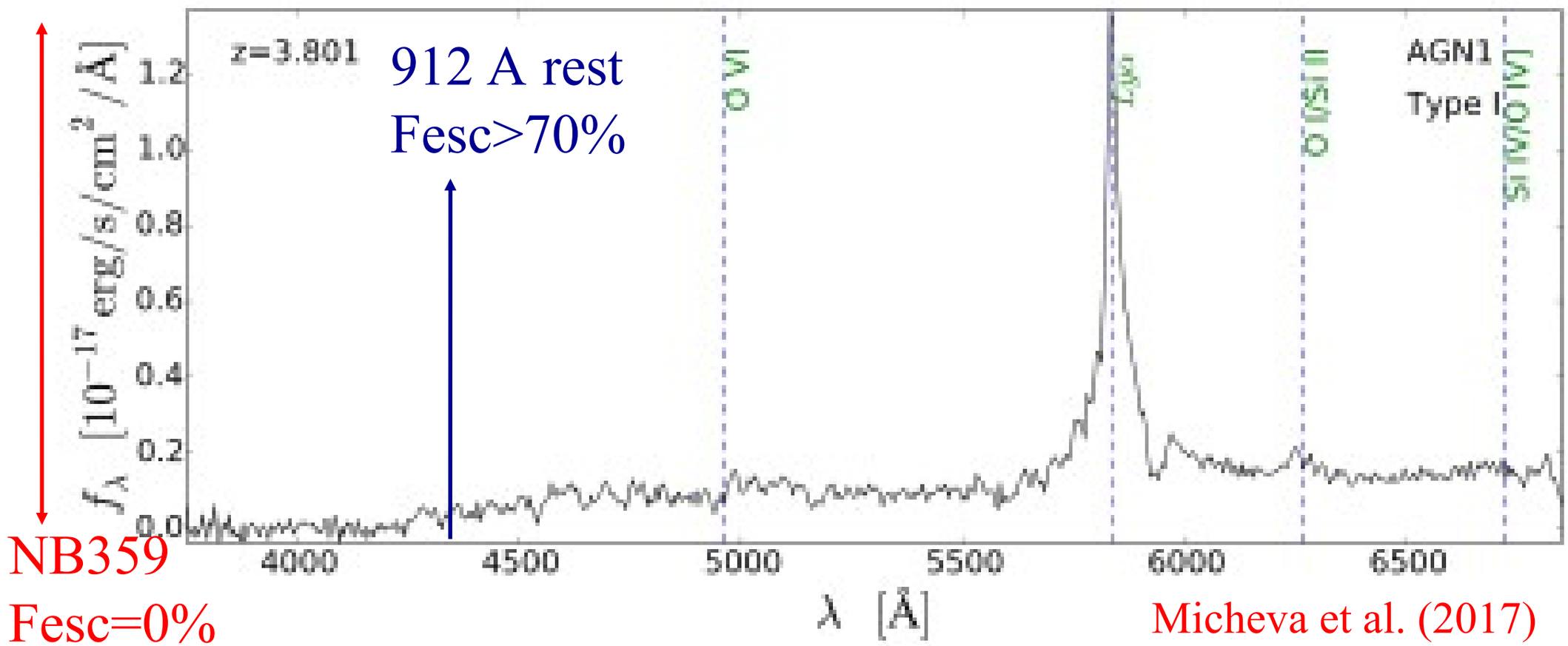

NB359 (LyC) is at 750 A rest frame (proper distance=173 pMpc).

The Mean free path at z=3.8 is 45 pMpc.

LyC fesc of z~3 AGN

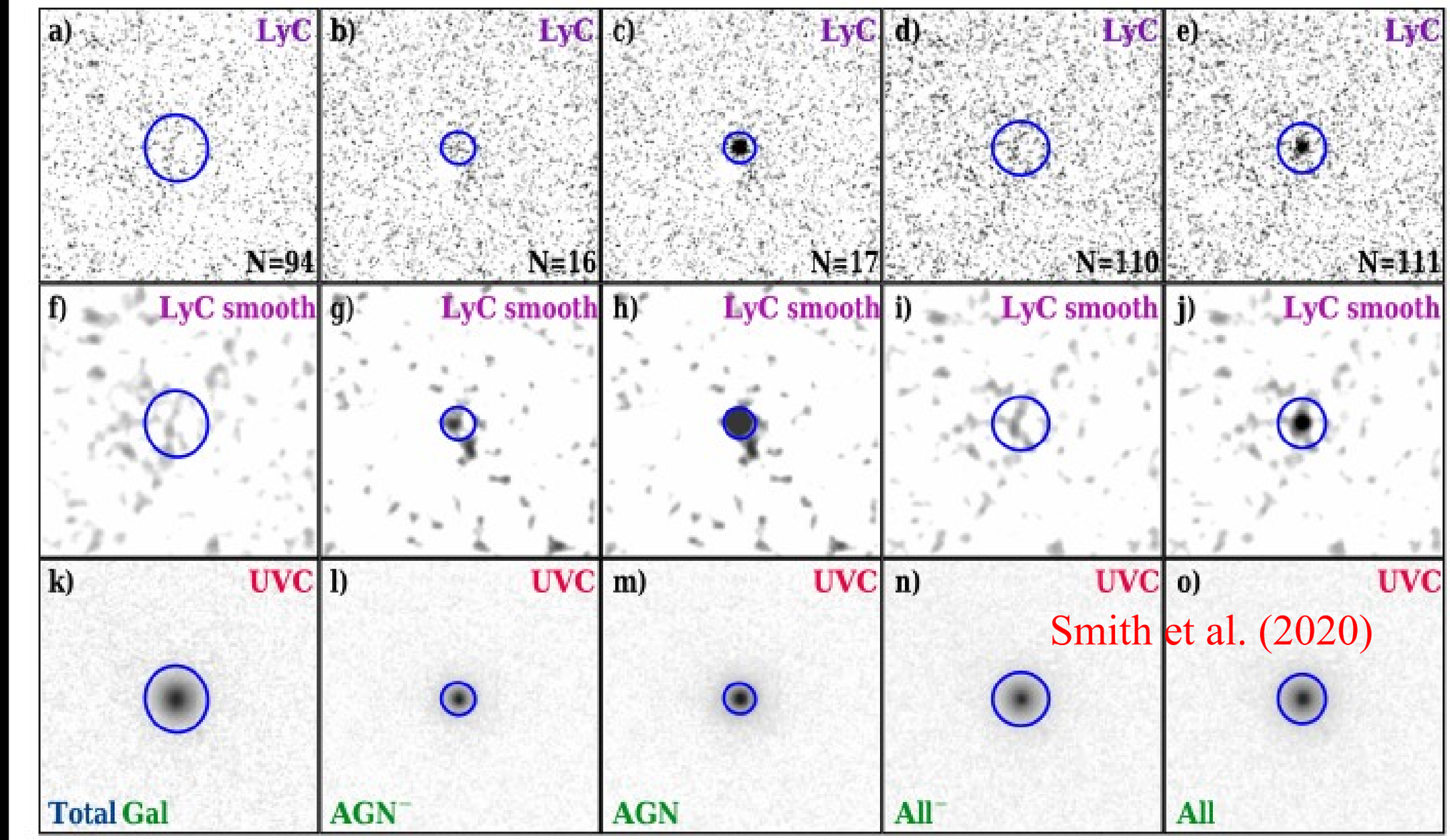

The stack of 17 AGN dominates the LyC production from z~2.3–4.3 by a factor of ~10 compared to all 94 galaxies without AGN. (See talk by R. Windhorst)

Low LyC fesc of faint AGN ?

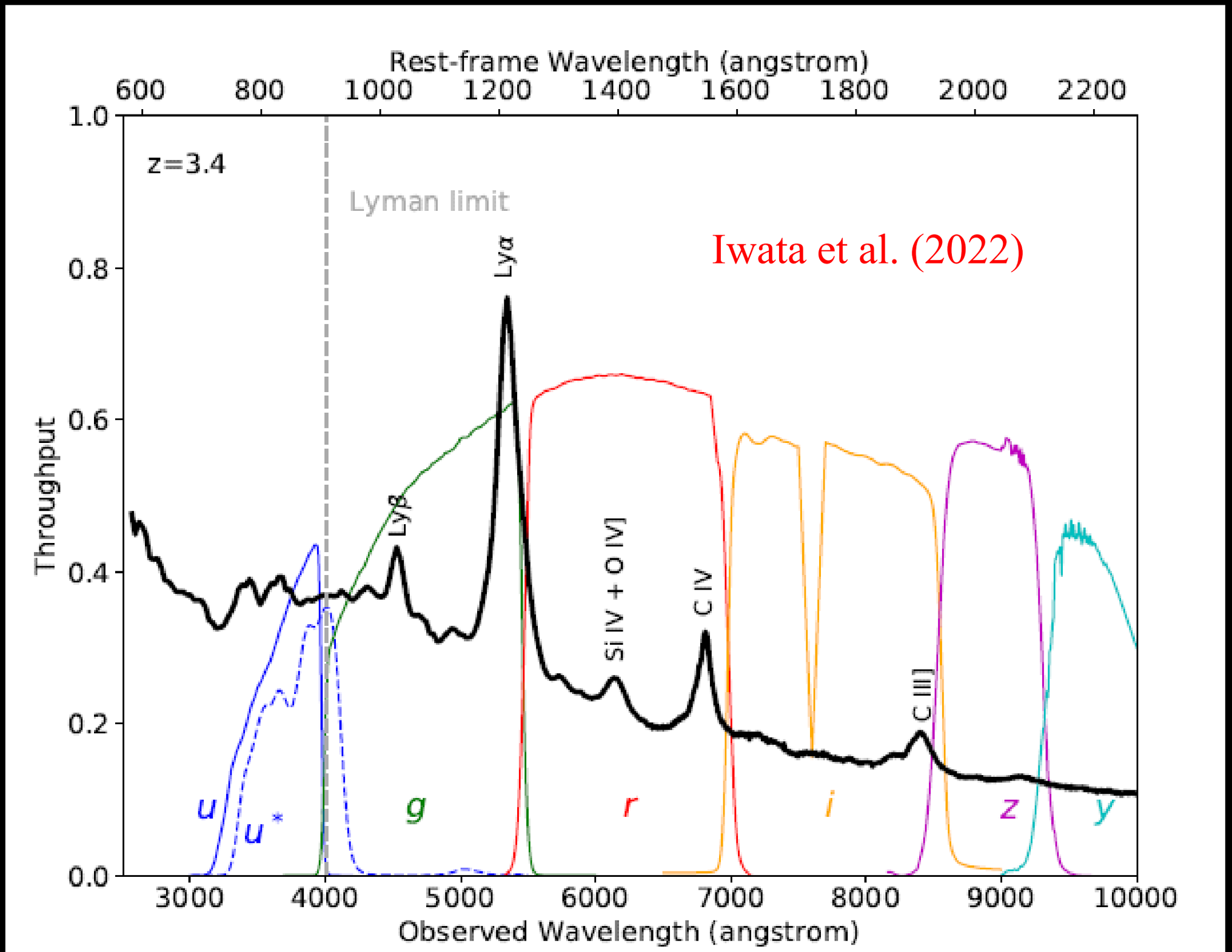

Faint High-z AGNs: low LyC fesc ?

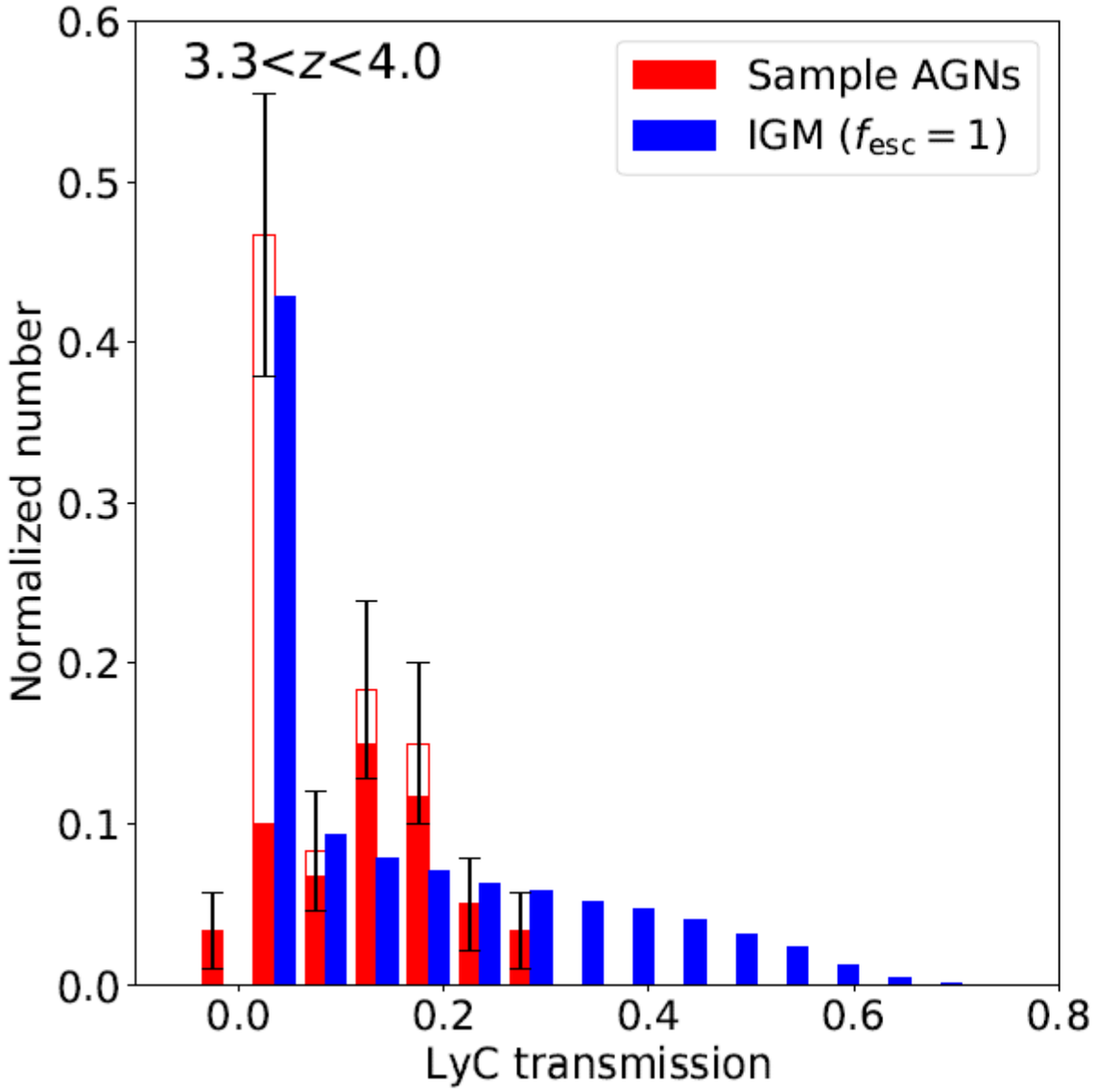

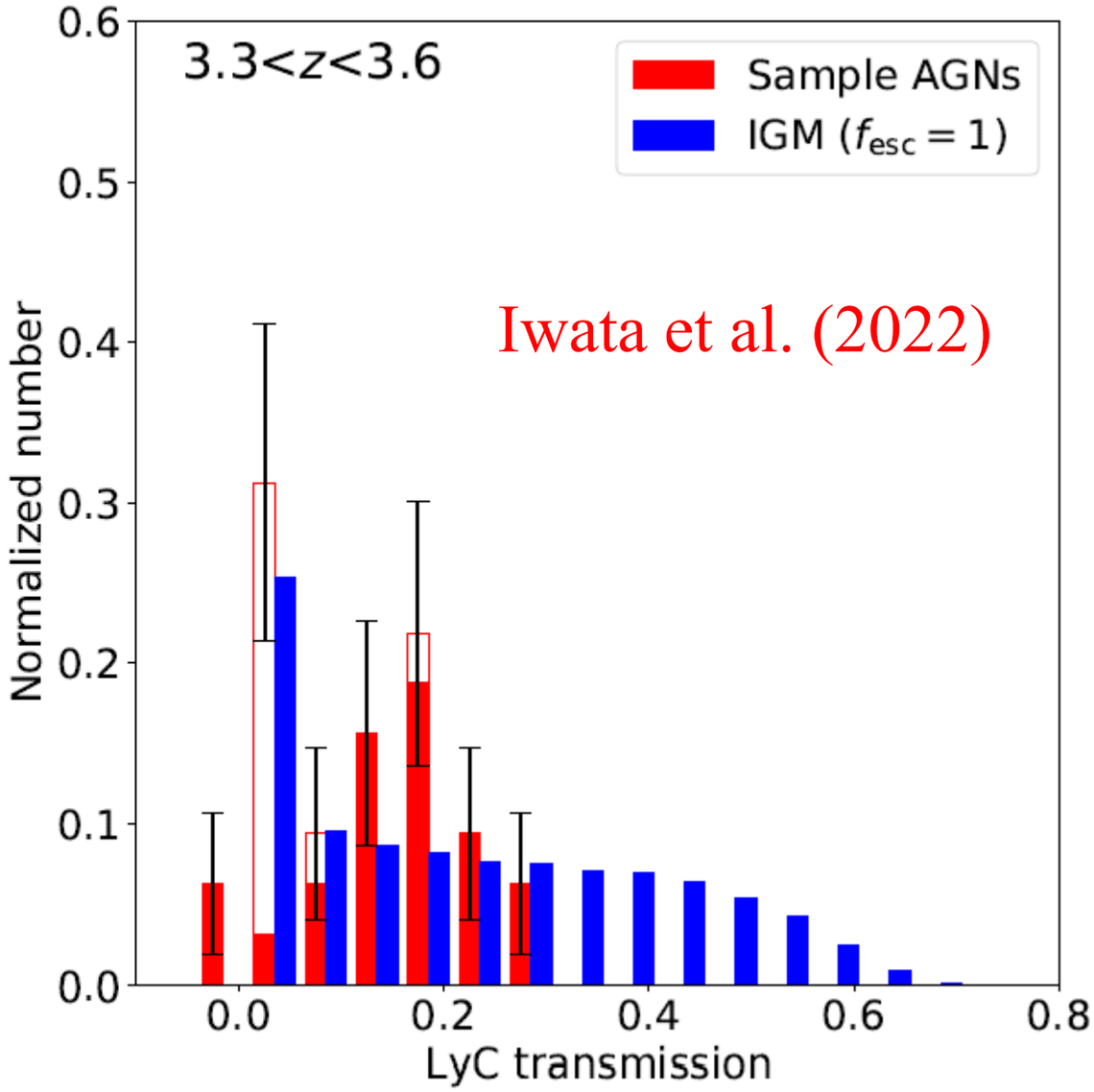

Iwata et al. (2022)

LyC fesc=25% for 94 faint (M1450>-24) AGNs at 3.3<z<4.0

COSMOS

Iwata et al. (2022)

ID	R.A.(J2000)	Decl.(J2000)	Redshift	M_{1450}	$U-i$	$t_{\rm Lyc}$	Filter	Type	N/E[a]	Ref.[b]	Designation
C07	149.4729034	2.7933720	3.6095	-24.127	3.18 ± 0.01	0.116 ± 0.000	u	BLA	N	09,09	COSMOS_J095753.49+024736.1
C08	149.5337247	1.8091995	3.9860	-23.357	> 5.54	< 0.015	u	–	N	10,–	B18_0664641
C10	149.6258478	1.9812633	3.9600	-20.957	2.15 ± 0.12	0.339 ± 0.013	u	BLA	E	11,11	L450105
C11	149.6959527	2.6030866	3.3030	-21.326	> 3.95	< -0.007	u	NLA	N	11,11	lid_1808
C12	149.7554065	2.7385464	3.5240	-22.169	> 4.55	< 0.032	u	BLA	E	12,09	COSMOS_J095901.31+024418.8
C13	149.7820781	2.4712961	3.3260	-21.819	> 4.33	< 0.003	u	BLA	N	11,11	L772453
C14	149.8432151	2.6590580	3.7480	-22.137	> 4.64	< 0.032	u	BLA	N	10,10	B18_1730531
C15	149.8457518	2.4816180	3.3600	-21.927	> 4.42	< 0.022	u	BLA	N	13,13	M12_1511846
C16	149.8458637	2.8604351	3.6300	-22.878	> 5.13	< 0.019	u	BLA	N	10,10	B18_1938843
C17	149.8494778	2.8652090	3.6860	-21.854	> 4.07	< 0.053	u	NLA	E	11,11	lid_2189
C18	149.8515634	2.2764026	3.3710	-22.412	2.45 ± 0.03	0.202 ± 0.001	u	BLA	N	12,12	XMMC_149.85099+2.27609
C19	149.8696906	2.2940175	3.3450	-23.675	> 6.24	< -0.010	u	BLA	N	12,12	XMMC_149.86981+2.29391
C20	149.8792145	2.2258072	3.6510	-23.017	> 5.42	< 0.015	u	BLA	N	12,12	XMMC_149.87949+2.22567
C21	149.8861225	2.2759378	3.3350	-21.944	> 4.52	< 0.005	u	NLA	E	11,11	cid_1134
C22	149.8942870	2.4329414	3.3600	-21.393	> 3.88	< 0.043	u	BLA	N	14,13	L747071
C23	149.9173822	2.8820631	3.3170	-21.920	2.40 ± 0.05	0.178 ± 0.006	u	BLA	N	14,14	L1040434
C24	150.0043858	2.0388885	3.4990	-24.064	3.24 ± 0.01	0.104 ± 0.000	u	BLA	N	12,12	XMMC_150.00412+2.03904
C25	150.0229091	1.5862527	3.3430	-21.297	2.49 ± 0.08	0.182 ± 0.004	u	NLA	E	11,11	lid_1244
C26	150.0426727	1.8721154	3.3600	-21.882	> 3.81	< 0.047	u	BLA	N	13,13	PRIMUS_110535
C27	150.0968272	2.0214452	3.5460	-20.424	> 2.68	< 0.180	u	NLA	E	15,15	CCOS1505
C28	150.1139556	2.6067261	3.9490	-20.793	> 2.72	< 0.198	u	BLA	E	14,14	L862385
C29	150.1164373	1.9638991	3.4100	-21.686	> 4.01	< 0.050	u	BLA	N	13,13	M12_0790476
C30	150.1303590	2.4659748	3.8650	-22.764	> 4.80	< 0.028	u	BLA	N	14,13	L768961
C31	150.2088406	2.4819033	3.3330	-25.774	> 8.15	< -0.027	u	BLA	N	12,12	XMMC_150.20888+2.48202
C32	150.2089844	2.4384687	3.7150	-24.470	> 6.64	< 0.005	u	BLA	N	12,12	XMMC_150.20929+2.43844
C33	150.2407920	2.6590184	3.3560	-22.578	2.56 ± 0.02	0.172 ± 0.001	u	BLA	N	12,09	XMMC_150.24087+2.65873
C34	150.2518296	1.5535407	3.7470	-21.494	> 3.31	< 0.108	u	BLA	N	14,14	L179154
C35	150.2595269	2.3761549	3.7170	-23.402	4.66 ± 0.10	0.031 ± 0.000	u	BLA	N	11,13	M12_1208399
C36	150.2630206	2.5208549	3.7580	-21.376	> 2.91	< 0.158	u	BLA	N	14,14	C1432719
C37	150.2671997	1.9096446	3.8460	-20.376	> 2.74	< 0.189	u	BLA	E	14,14	L405213
C38	150.2715836	1.6138443	3.5120	-20.122	> 2.67	< 0.177	u	NLA	N	11,11	cid_1656
C39	150.2972445	2.1487816	3.3280	-25.123	4.48 ± 0.01	-0.001 ± 0.007	u	BLA	N	12,12	XMMC_150.29764+2.14830
C40	150.3007581	2.3005428	3.4980	-21.426	> 3.98	< 0.053	u	NLA	E	15,15	CCOS784
C41	150.3025734	1.8520637	3.8400	-21.044	> 3.42	< 0.101	u	BLA	N	13,13	L368476
C42	150.3060182	1.7616025	3.3100	-20.338	> 3.01	< 0.075	u	NLA	E	11,11	cid_3293
C43	150.3445675	1.6359393	3.4820	-19.177	> 1.69	< 0.431	u	NLA	E	11,11	cid_1672
C44	150.3647089	2.1437853	3.3280	-22.050	> 3.72	< 0.032	u	BLA	E	14,12	L554731
C45	150.3835833	2.0747463	3.8590	-20.999	> 3.19	< 0.125	u	–	E	16,–	CCOS879
C46	150.3941052	2.7178277	3.4870	-21.600	1.55 ± 0.03	0.492 ± 0.006	u	NLA	E	11,11	lid_4112
C47	150.4029080	1.8788719	3.5710	-20.394	1.84 ± 0.08	0.393 ± 0.012	u	NLA	E	11,11	cid_2949
C49	150.4399178	2.7034886	3.4650	-22.510	2.79 ± 0.03	0.155 ± 0.001	u	BLA	N	09,09	COSMOS_J100145.58+024212.6

Fesc=74% Grazian+18

Iwata et al. (2022)

COSMOS

ID	R.A.(J2000)	Decl.(J2000)	Redshift	M_{1450}	$U-i$	$t_{\rm Lyc}$	Filter	Type	N/E[a]	Ref.[b]	Designation
C07	149.4729034	2.7933720	3.6095	−24.127	3.18 ± 0.01	0.116 ± 0.000	u	BLA	N	09,09	COSMOS_J095753.49+024736.1
C08	149.5337247	1.8091995	3.9860	−23.357	> 5.54	< 0.015	u	–	N	10,–	B18_0664641
C10	149.6258478	1.9812633	3.9600	−20.957	2.15 ± 0.12	0.339 ± 0.013	u	BLA	E	11,11	L450105
C11	149.6959527	2.6030866	3.3030	−21.326	> 3.95	< -0.007	u	NLA	N	11,11	lid_1808
C12	149.7554065	2.7385464	3.5240	−22.169	> 4.55	< 0.032	u	BLA	E	12,09	COSMOS_J095901.31+024418.8
C13	149.7820781	2.4712961	3.3260	−21.819	> 4.33	< 0.003	u	BLA	N	11,11	L772453
C14	149.8432151	2.6590580	3.7480	−22.137	> 4.64	< 0.032	u	BLA	N	10,10	B18_1730531
C15	149.8457518	2.4816180	3.3600	−21.927	> 4.42	< 0.022	u	BLA	N	13,13	M12_1511846
C16	149.8458637	2.8604351	3.6300	−22.878	> 5.13	< 0.019	u	BLA	N	10,10	B18_1938843
C17	149.8494778	2.8652090	3.6860	−21.854	> 4.07	< 0.053	u	NLA	E	11,11	lid_2189
C18	149.8515634	2.2764026	3.3710	−22.412	2.45 ± 0.03	0.202 ± 0.001	u	BLA	N	12,12	XMMC_149.85099+2.27609
C19	149.8696906	2.2940175	3.3450	−23.675	> 6.24	< -0.010	u	BLA	N	12,12	XMMC_149.86981+2.29391
C20	149.8792145	2.2258072	3.6510	−23.017	> 5.42	< 0.015	u	BLA	N	12,12	XMMC_149.87949+2.22567
C21	149.8861225	2.2759378	3.3350	−21.944	> 4.52	< 0.005	u	NLA	E	11,11	cid_1134
C22	149.8942870	2.4329414	3.3600	−21.393	> 3.88	< 0.043	u	BLA	N	14,13	L747071
C23	149.9173822	2.8820631	3.3170	−21.920	2.40 ± 0.05	0.178 ± 0.006	u	BLA	N	14,14	L1040434
C24	150.0043858	2.0388885	3.4990	−24.064	3.24 ± 0.01	0.104 ± 0.000	u	BLA	N	12,12	XMMC_150.00412+2.03904
C25	150.0229091	1.5862527	3.3430	−21.297	2.49 ± 0.08	0.182 ± 0.004	u	NLA	E	11,11	lid_1244
C26	150.0426727	1.8721154	3.3600	−21.882	> 3.81	< 0.047	u	BLA	N	13,13	PRIMUS_110535
C27	150.0968272	2.0214452	3.5460	−20.424	> 2.68	< 0.180	u	NLA	E	15,15	CCOS1505
C28	150.1139556	2.6067261	3.9490	−20.793	> 2.72	< 0.198	u	BLA	E	14,14	L862385
C29	150.1164373	1.9638991	3.4100	−21.686	> 4.01	< 0.050	u	BLA	N	13,13	M12_0790476
C30	150.1303590	2.4659748	3.8650	−22.764	> 4.80	< 0.028	u	BLA	N	14,13	L768961
C31	150.2088406	2.4819033	3.3330	−25.774	> 8.15	< -0.027	u	BLA	N	12,12	XMMC_150.20888+2.48202
C32	150.2089844	2.4384687	3.7150	−24.470	> 6.64	< 0.005	u	BLA	N	12,12	XMMC_150.20929+2.43844
C33	150.2407920	2.6590184	3.3560	−22.578	2.56 ± 0.02	0.172 ± 0.001	u	BLA	N	12,09	XMMC_150.24087+2.65873
C34	150.2518296	1.5535407	3.7470	−21.494	> 3.31	< 0.108	u	BLA	N	14,14	L179154
C35	150.2595269	2.3761549	3.7170	−23.402	4.66 ± 0.10	0.031 ± 0.000	u	BLA	N	11,13	M12_1208399
C36	150.2630206	2.5208549	3.7580	−21.376	> 2.91	< 0.158	u	BLA	N	14,14	C1432719
C37	150.2671997	1.9096446	3.8460	−20.376	> 2.74	< 0.189	u	BLA	E	14,14	L405213
C38	150.2715836	1.6138443	3.5120	−20.122	> 2.67	< 0.177	u	NLA	N	11,11	cid_1656
C39	150.2972445	2.1487816	3.3280	−25.123	4.48 ± 0.01	-0.001 ± 0.007	u	BLA	N	12,12	XMMC_150.29764+2.14830
C40	150.3007581	2.3005428	3.4980	−21.426	> 3.98	< 0.053	u	NLA	E	15,15	CCOS784
C41	150.3025734	1.8520637	3.8400	−21.044	> 3.42	< 0.101	u	BLA	N	13,13	L368476
C42	150.3060182	1.7616025	3.3100	−20.338	> 3.01	< 0.075	u	NLA	E	11,11	cid_3293
C43	150.3445675	1.6359393	3.4820	−19.177	> 1.69	< 0.431	u	NLA	E	11,11	cid_1672
C44	150.3647089	2.1437853	3.3280	−22.050	> 3.72	< 0.032	u	BLA	E	14,12	L554731
C45	150.3835833	2.0747463	3.8590	−20.999	> 3.19	< 0.125	u	–	E	16,–	CCOS879
C46	150.3941052	2.7178277	3.4870	−21.600	1.55 ± 0.03	0.492 ± 0.006	u	NLA	E	11,11	lid_4112
C47	150.4029080	1.8788719	3.5710	−20.394	1.84 ± 0.08	0.393 ± 0.012	u	NLA	E	11,11	cid_2949
C49	150.4399178	2.7034886	3.4650	−22.510	2.79 ± 0.03	0.155 ± 0.001	u	BLA	N	09,09	COSMOS_J100145.58+024212.6

Fesc=51% Grazian+18

Fesc=51% Grazian+18

Fesc=78% Grazian+18

Iwata et al. (2022)

COSMOS											
ID	R.A.(J2000)	Decl.(J2000)	Redshift	M_{1450}	$U-i$	$t_{\rm Lyc}$	Filter	Type	N/E[a]	Ref.[b]	Designation
C50	150.4549406	1.9673839	3.4710	−21.548	> 3.96	< 0.053	u	BLA	N	11,11	L441487
C51	150.5508002	2.6828885	3.5600	−21.818	> 4.11	< 0.048	u	BLA	N	13,13	M12_1628943
C52	150.6384404	2.3913200	3.6500	−23.195	> 5.04	< 0.021	u	BLA	N	13,13	M12_1159815
C53	150.7037829	2.3699723	3.7490	−23.966	3.28 ± 0.02	0.112 ± 0.000	u	BLA	N	12,12	XMMC_150.70394+2.36961
C54	150.7170733	1.9301231	3.5675	−22.732	1.23 ± 0.01	0.694 ± 0.003	u	BLA	E	11,11	L419634
C55	150.7355581	2.1995513	3.4970	−25.257	3.14 ± 0.00	0.063 ± 0.006	u^*	BLA	N	11,12	lid_1710
C56	150.7371767	2.7225658	3.3020	−23.399	2.29 ± 0.01	0.186 ± 0.009	u	BLA	N	12,09	COSMOS_J100256.92+024321.2
C57	150.7822171	2.2850682	3.6260	−23.993	3.79 ± 0.03	0.046 ± 0.001	u^*	BLA	N	10,10	B18_0899256
C59	150.8013187	1.6574845	3.7720	−23.212	> 5.63	< 0.013	u	–	N	10,–	B18_0247934
C60	150.9112639	1.9448424	3.6800	−24.963	4.43 ± 0.02	0.038 ± 0.000	u	BLA	N	03,03	VVDSWIDE:100359356
C61	150.9430180	1.3197523	3.5570	−24.265	> 6.63	< 0.005	u	BLA	N	03,03	VVDSWIDE:100105943
C62	151.2614791	1.4073308	3.4035	−25.349	3.07 ± 0.00	0.117 ± 0.000	u	BLA	N	02,02	SDSS100502.75+012426.3

Name	Iwata+22	Grazian+18
C07	fesc=19%	fesc=74%
C32	fesc<1%	fesc=51%
C35	fesc=5%	fesc=51%
C53	fesc=18%	fesc=78%

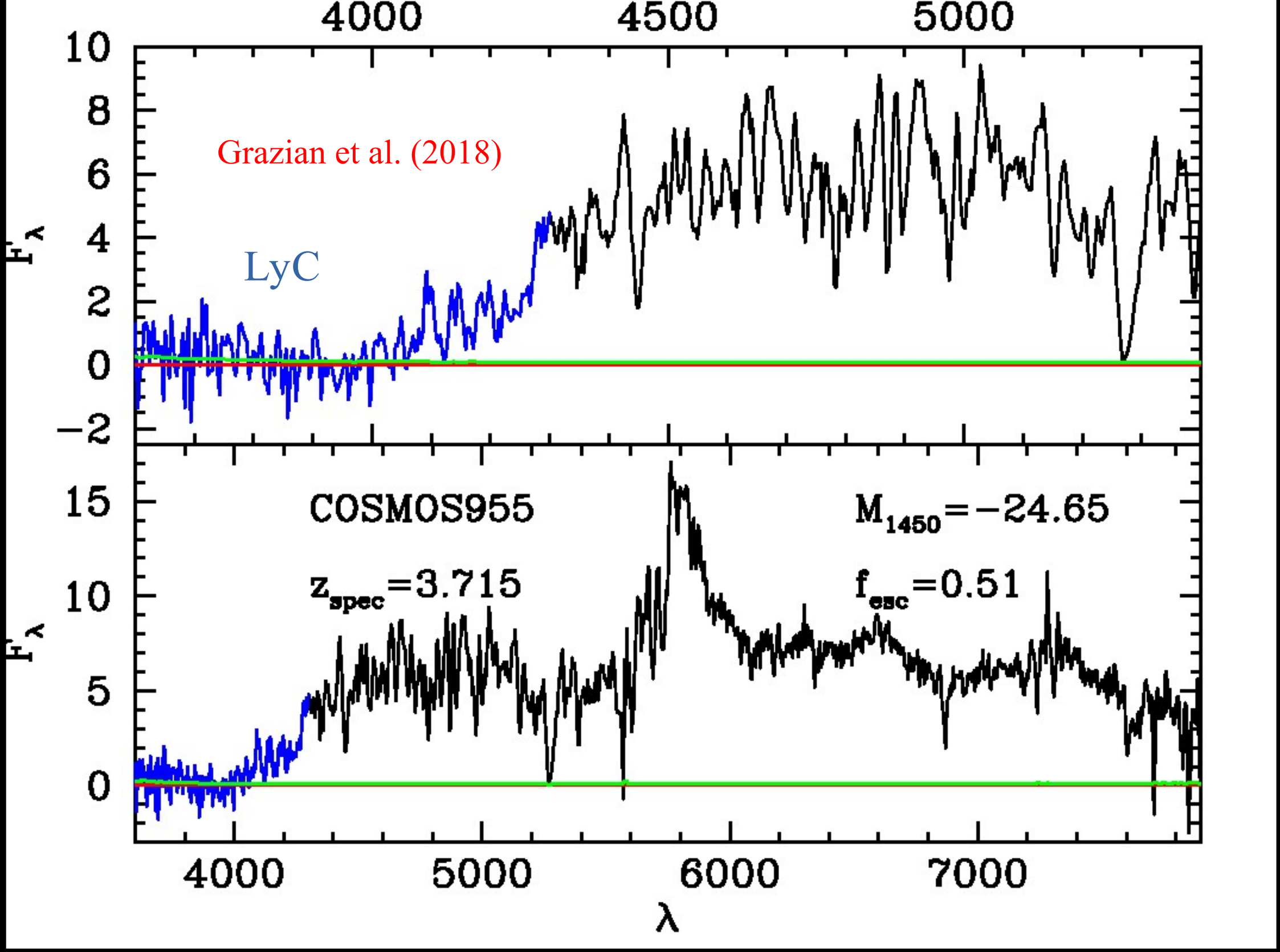

Name Iwata+22 Grazian+18

C32 fesc<1% fesc=51%

AGN LyC fesc from spectra

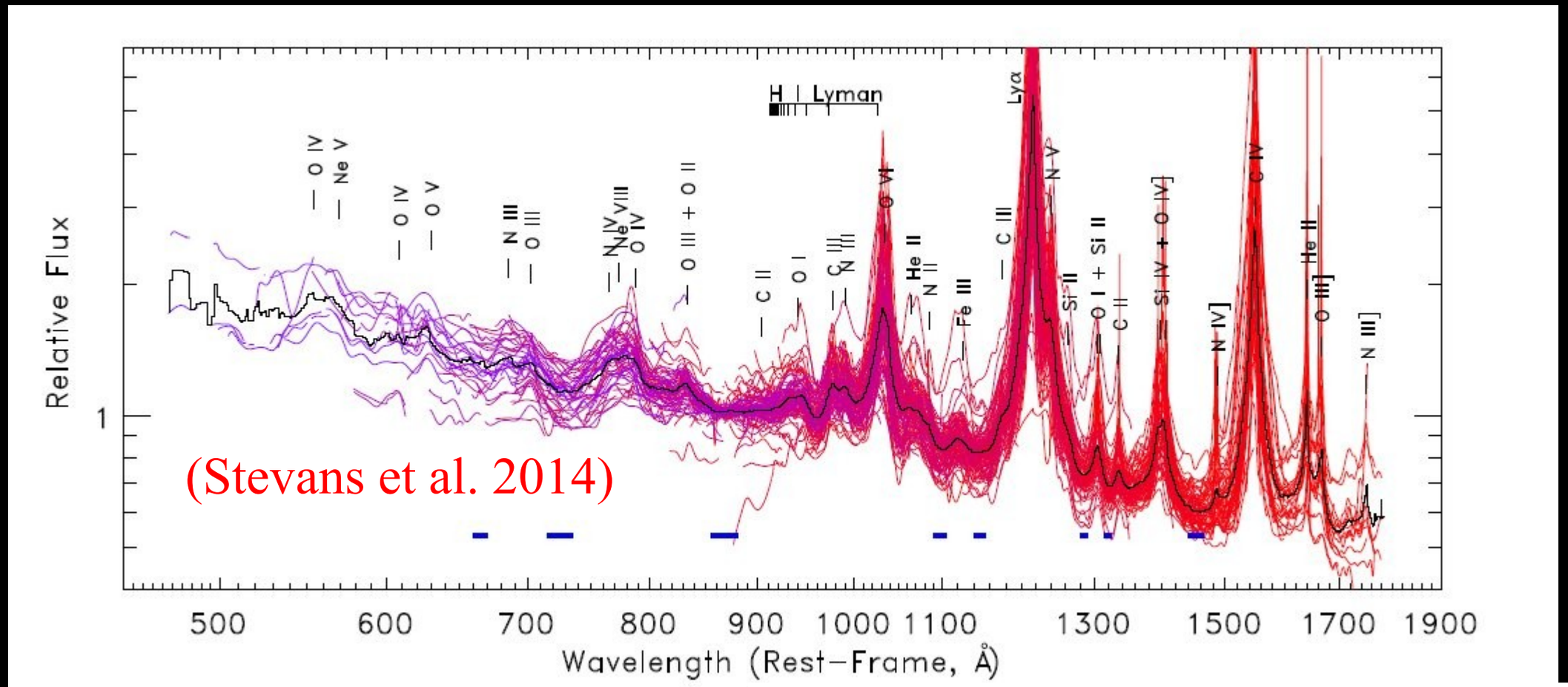

Stevans et al. (2014) find significant LyC emission in 159 low-luminosity AGNs at z<1.5

(both type 1 and type 1.8-1.9 AGNs)

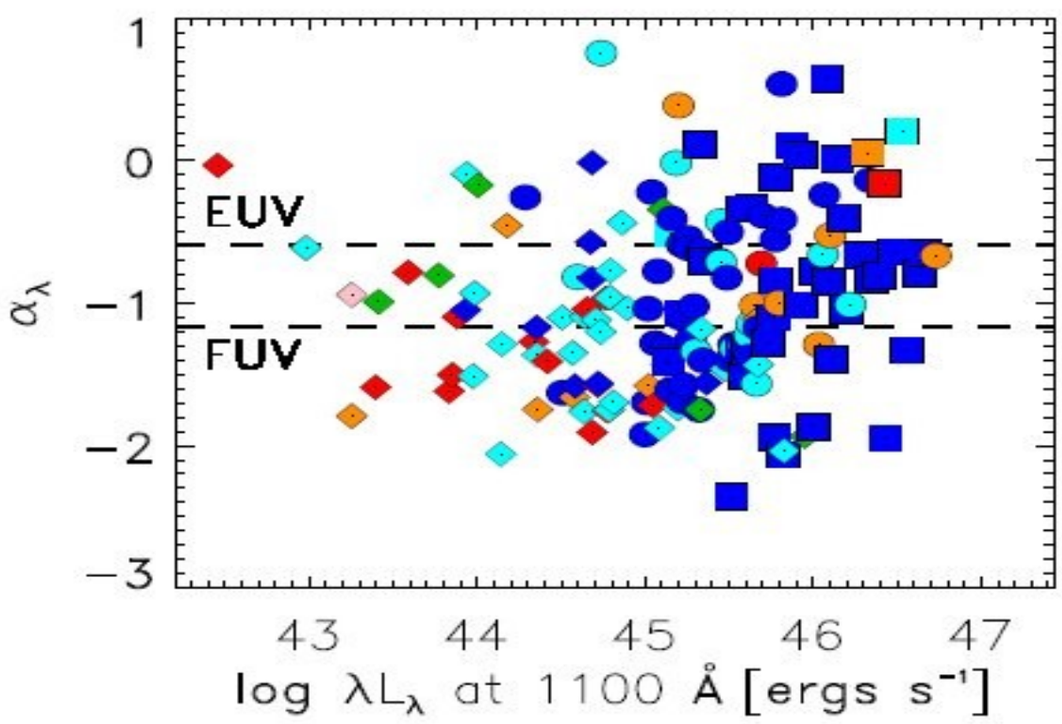

Very bright QSOs show high fesc

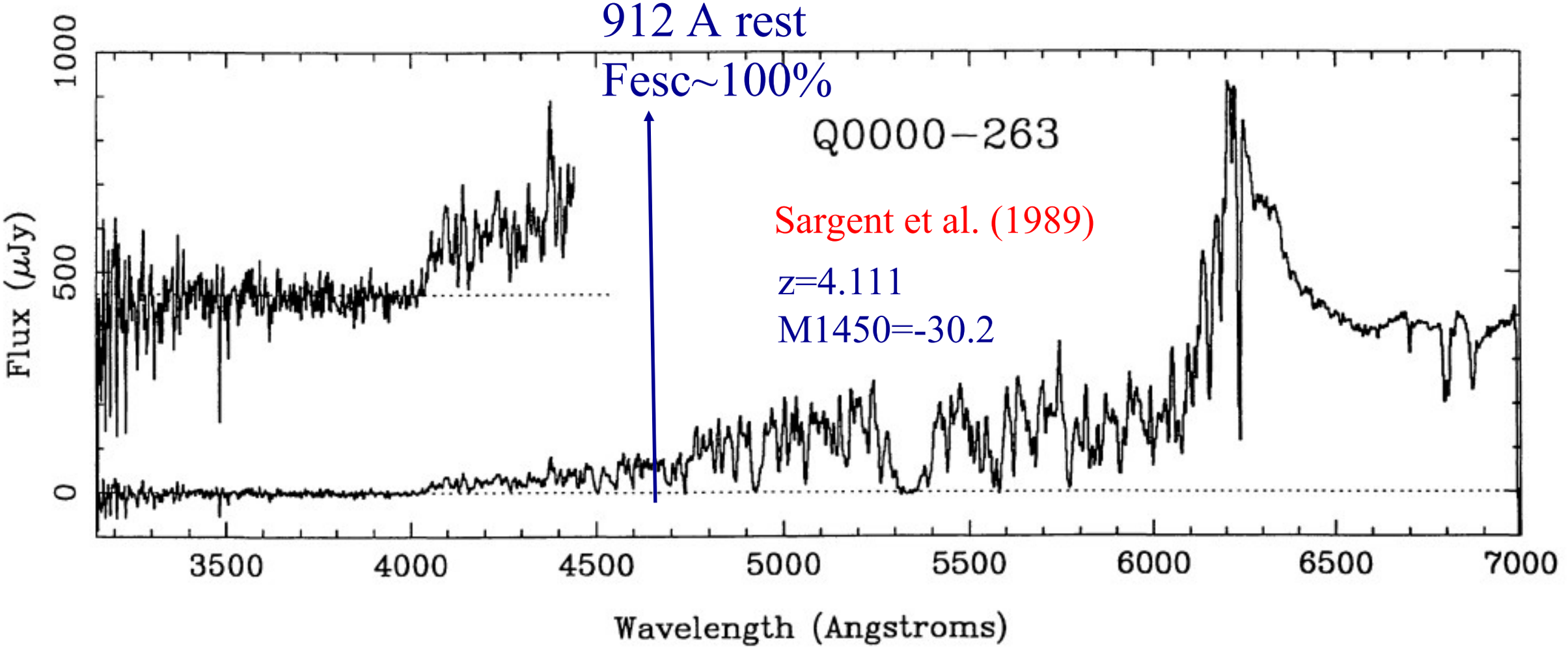

LyC emission of high-z QSOs

Bright high-z QSOs are strong LyC emitters

Direct detection of LyC up to z=5.5

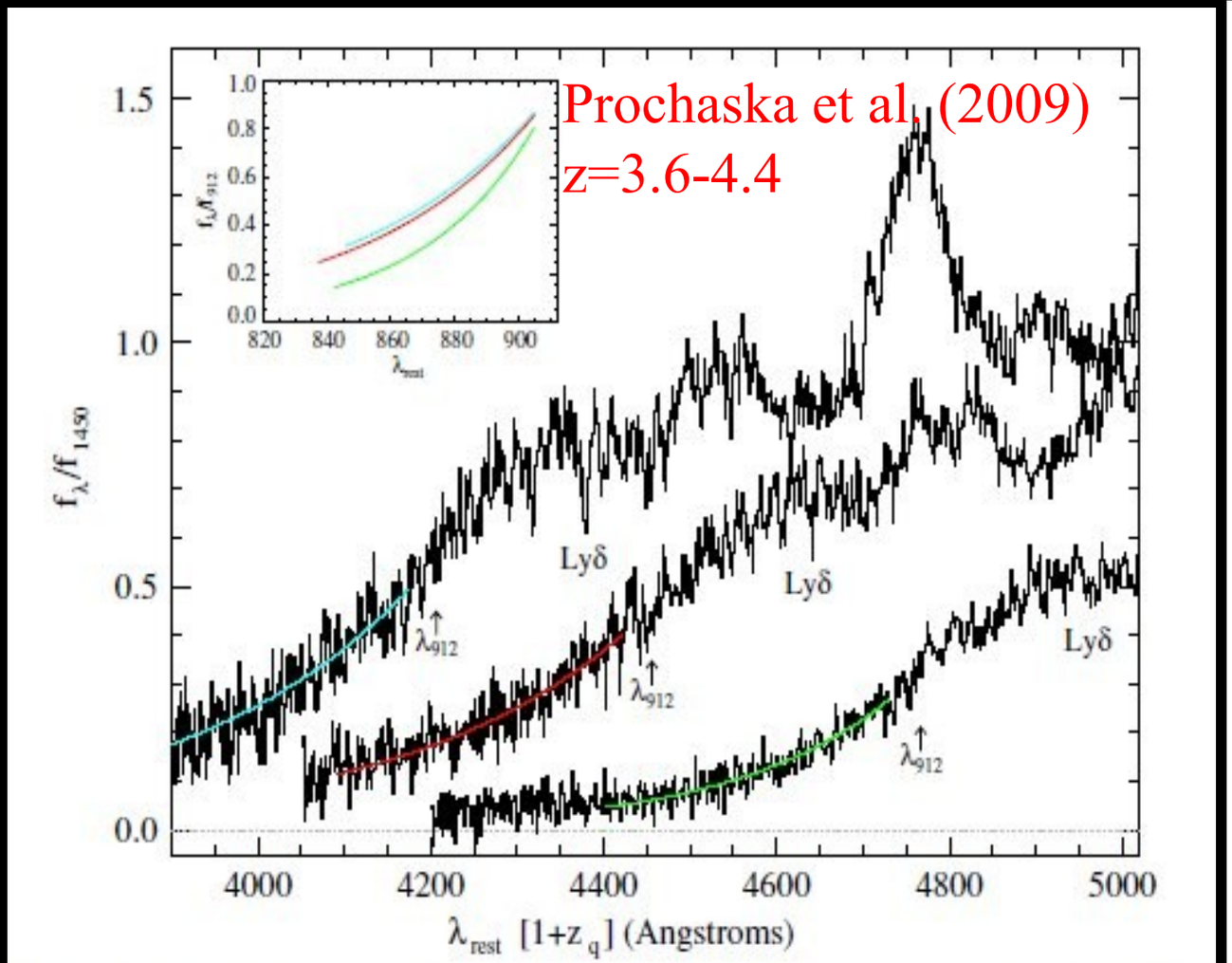

Figure 2. Stacked spectrum for three of our redshift bins (cyan: $z = [3.59, 3.63]$; red: $z = [3.86, 3.92]$; green: $z = [4.13, 4.34]$) plotted against rest-frame wavelengths redshifted to the mean quasar redshift for the bin. Overplotted on each spectrum is our best-fit model for the absorbed flux below λ_{912} due to the Lyman limit opacity. These same curves are shown in the sub-panel against rest wavelengths. The emission lines are from Lyman series and metal-line transitions.

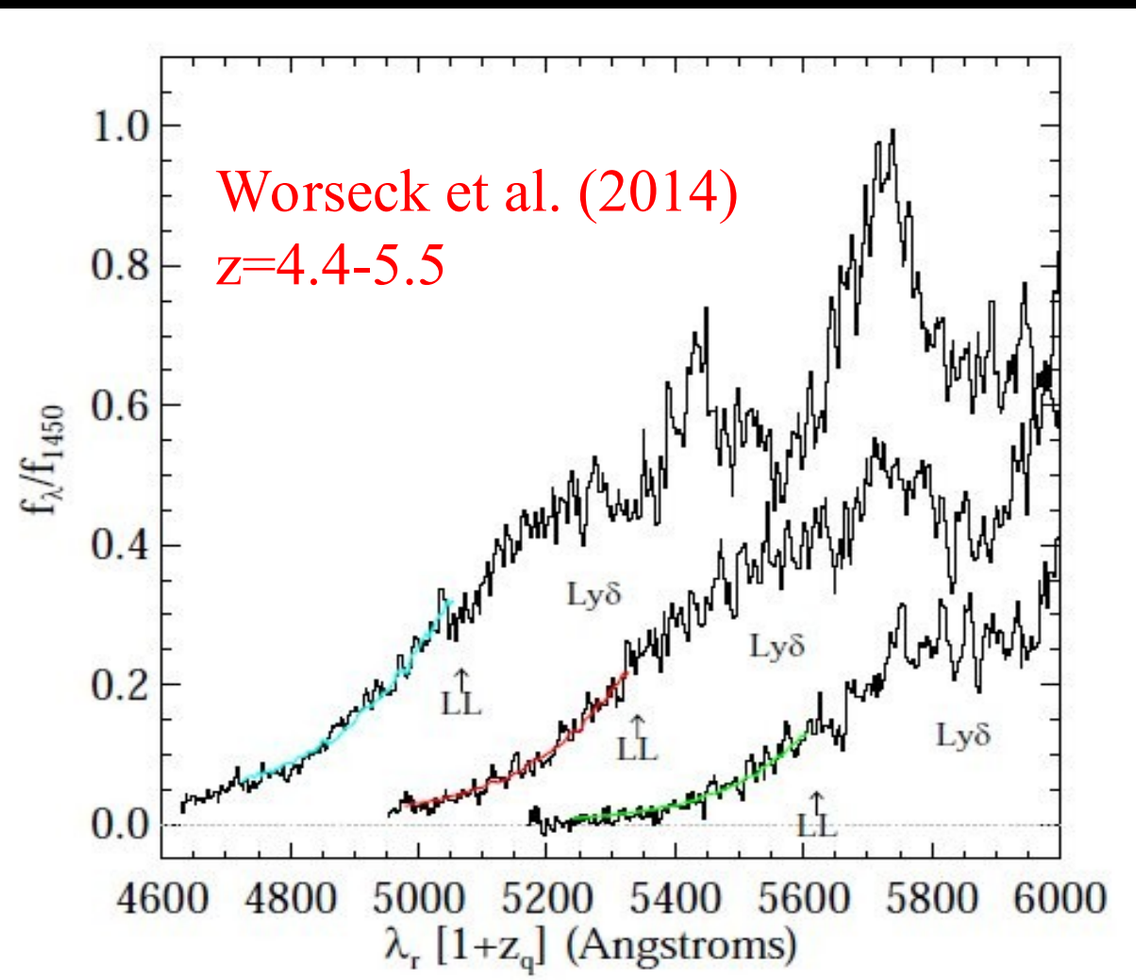

Figure 6. Stacked normalized rest-frame quasar spectra from the GGG survey generated for three redshift intervals: $z_{\rm em} = [4.4, 4.7]$, $[4.7, 5.0]$, and $[5.0, 5.5]$. These spectra are plotted in a pseudo-observer frame defined as $\lambda_{\rm r}\,(1 + z_{\rm q})$ with, $z_{\rm q}$ the average redshift of the quasars in each interval. The Lyδ emission (strongly affected by IGM absorption for the two high-z bins) and the onset of the Lyman limit are marked for each stacked spectrum. Lyβ and Lyγ emission lines of the background quasars are clearly visible. Overplotted on these stacked spectra are the best-fitting models which provide measurements for the mean free path $\lambda_{\rm mfp}^{912}$.

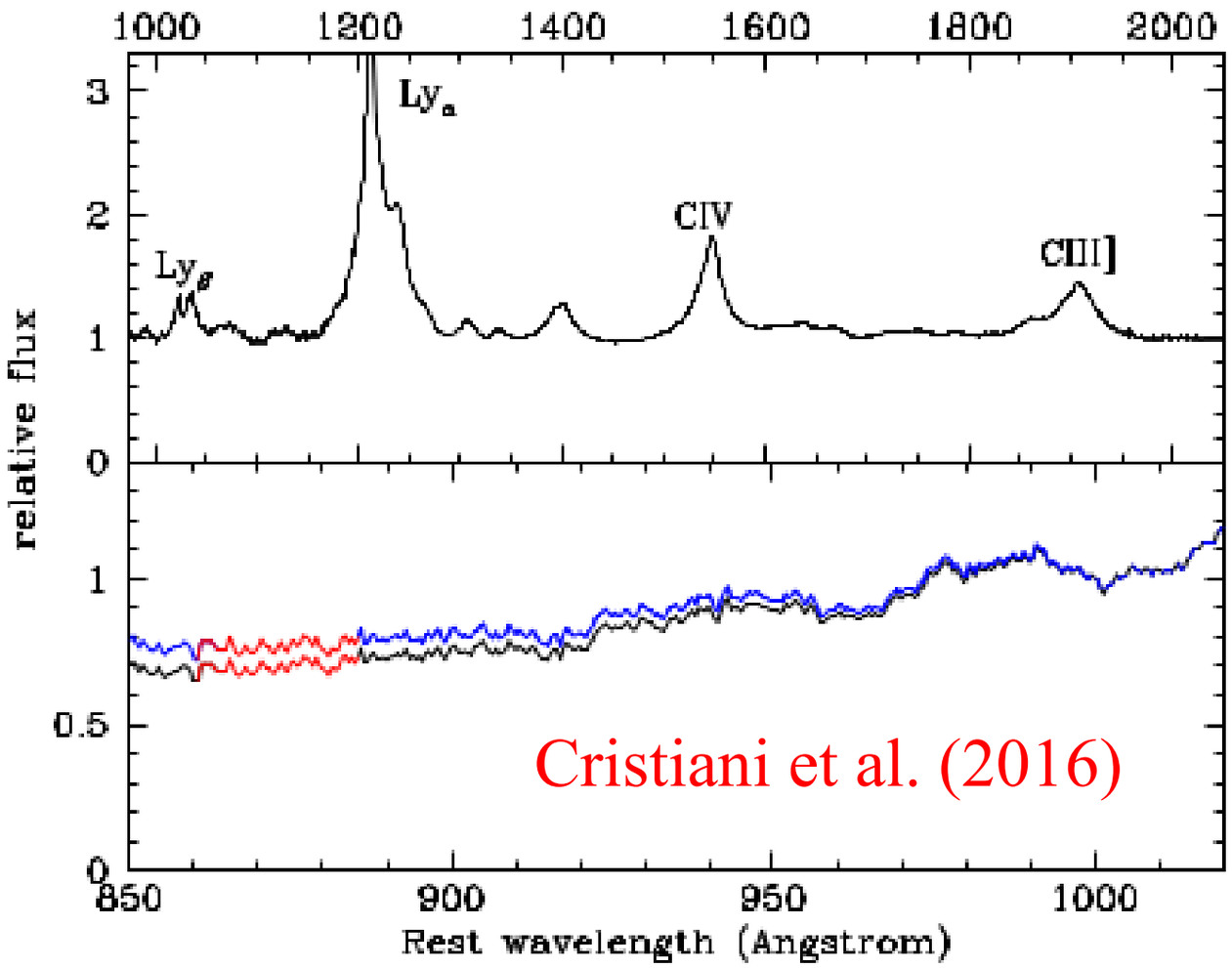

Cristiani et al. (2016)

LyC fesc>=75% for QSOs at 3.6<z<4.0 and M1450<-26

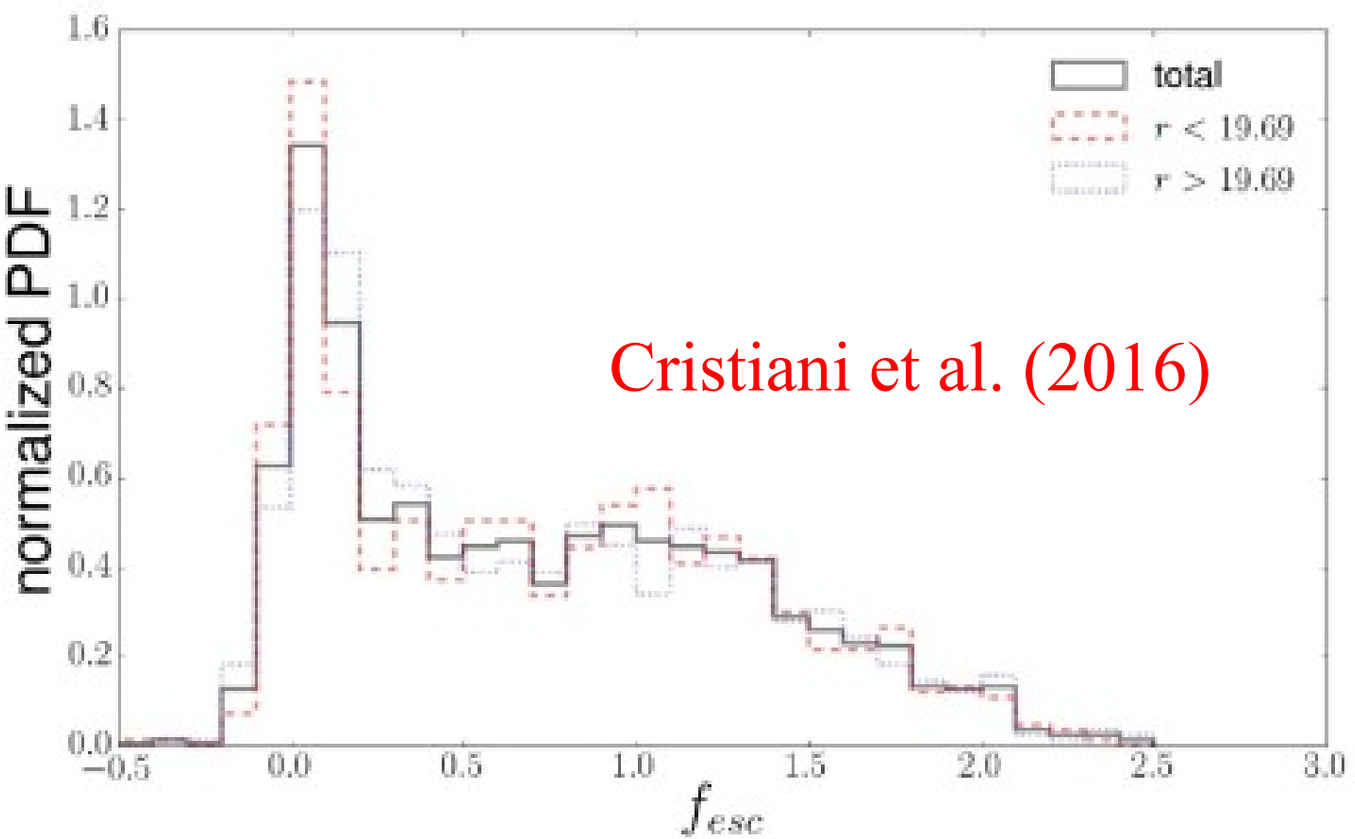

Cristiani et al. (2016)

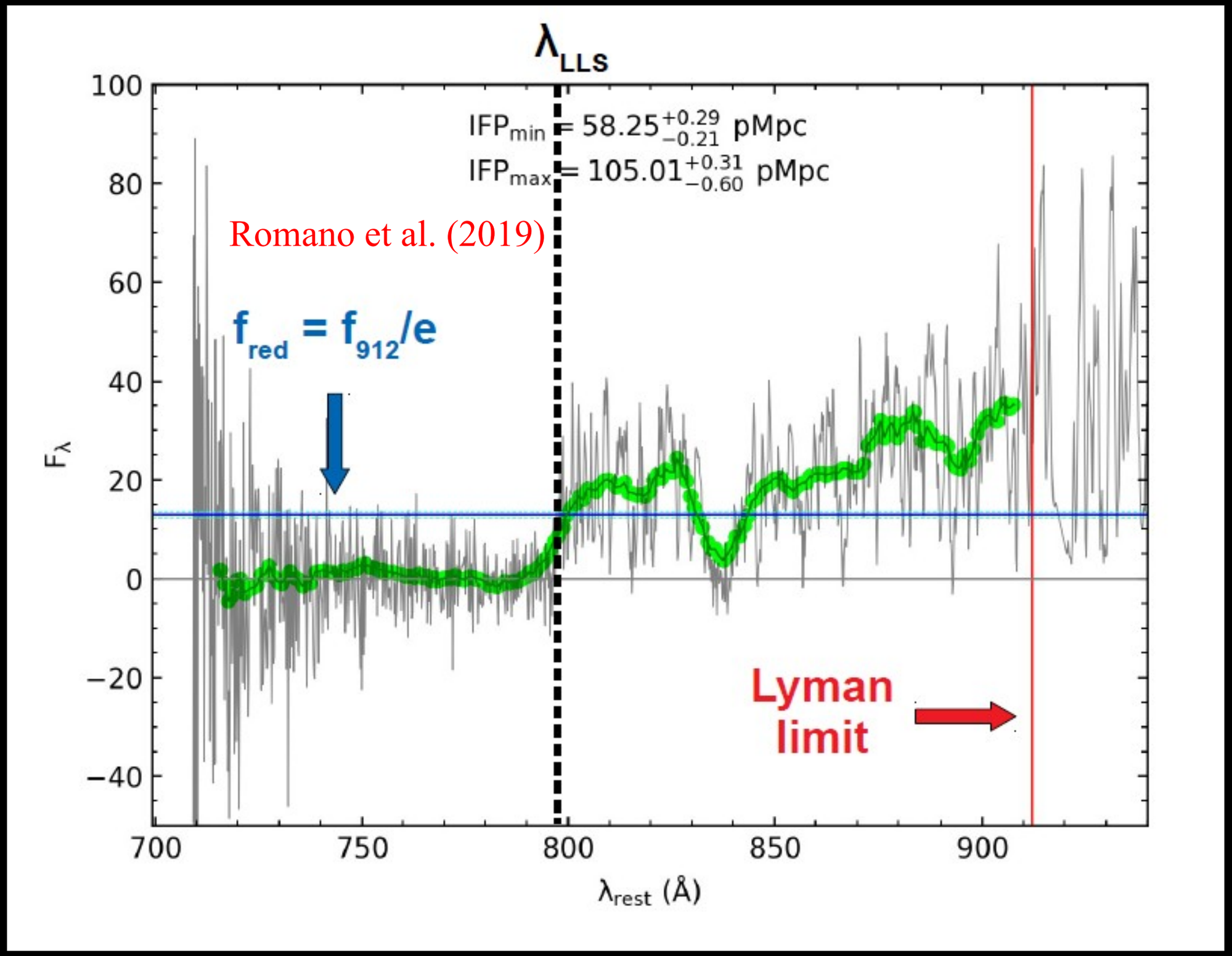
λLLS
IFPmin = 58.25+0.29−0.21 pMpc
IFPmax = 105.01+0.31−0.60 pMpc
Romano et al. (2019)
f_red = f_912/e
Lyman limit
Fλ
λrest (Å)
100
80
60
40
20
0
−20
−40
700
750
800
850
900

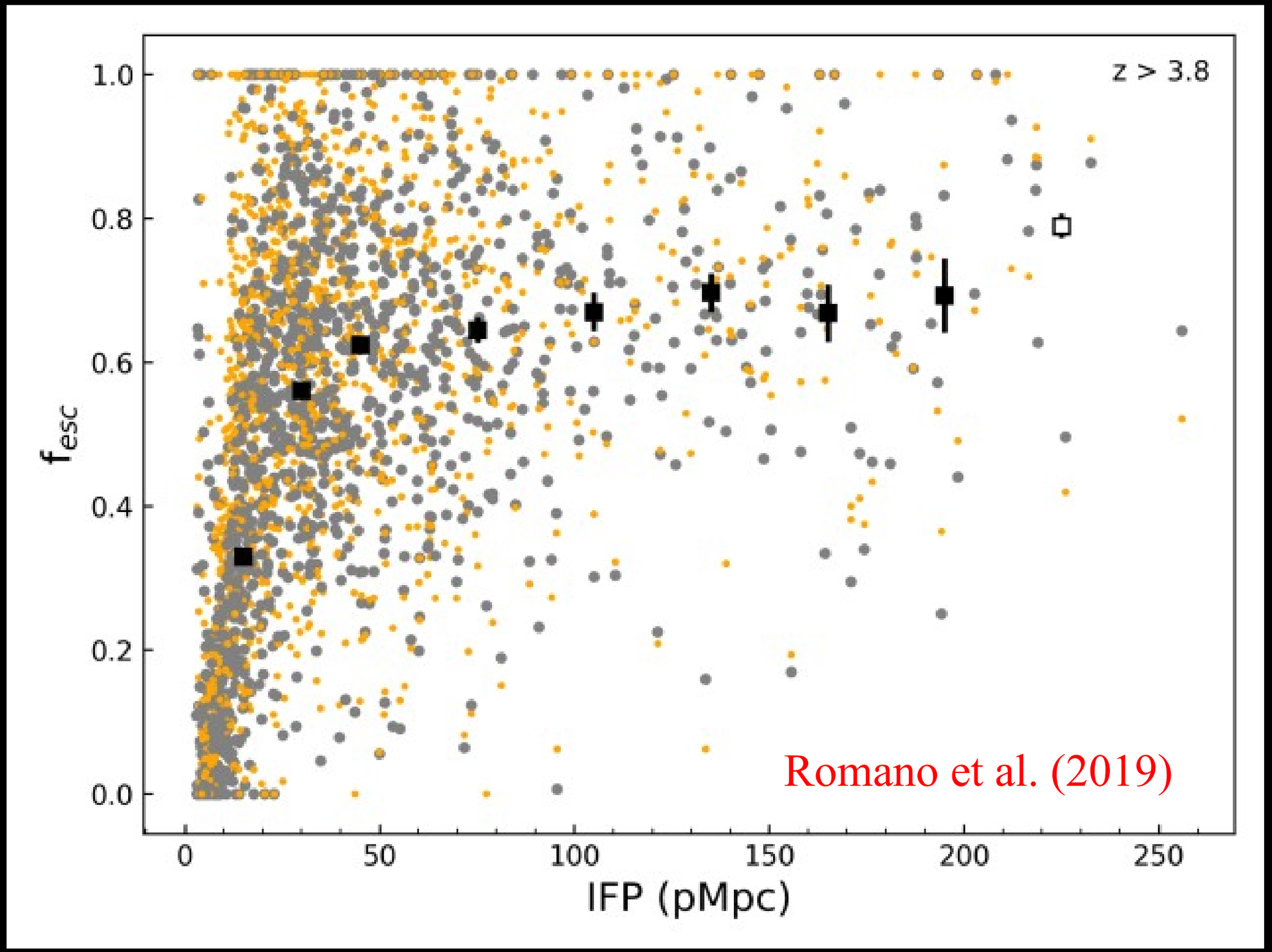
z > 3.8
1.0
0.8
0.6
0.4
0.2
0.0
f_{esc}
0
50
100
150
200
250
IFP (pMpc)
Romano et al. (2019)

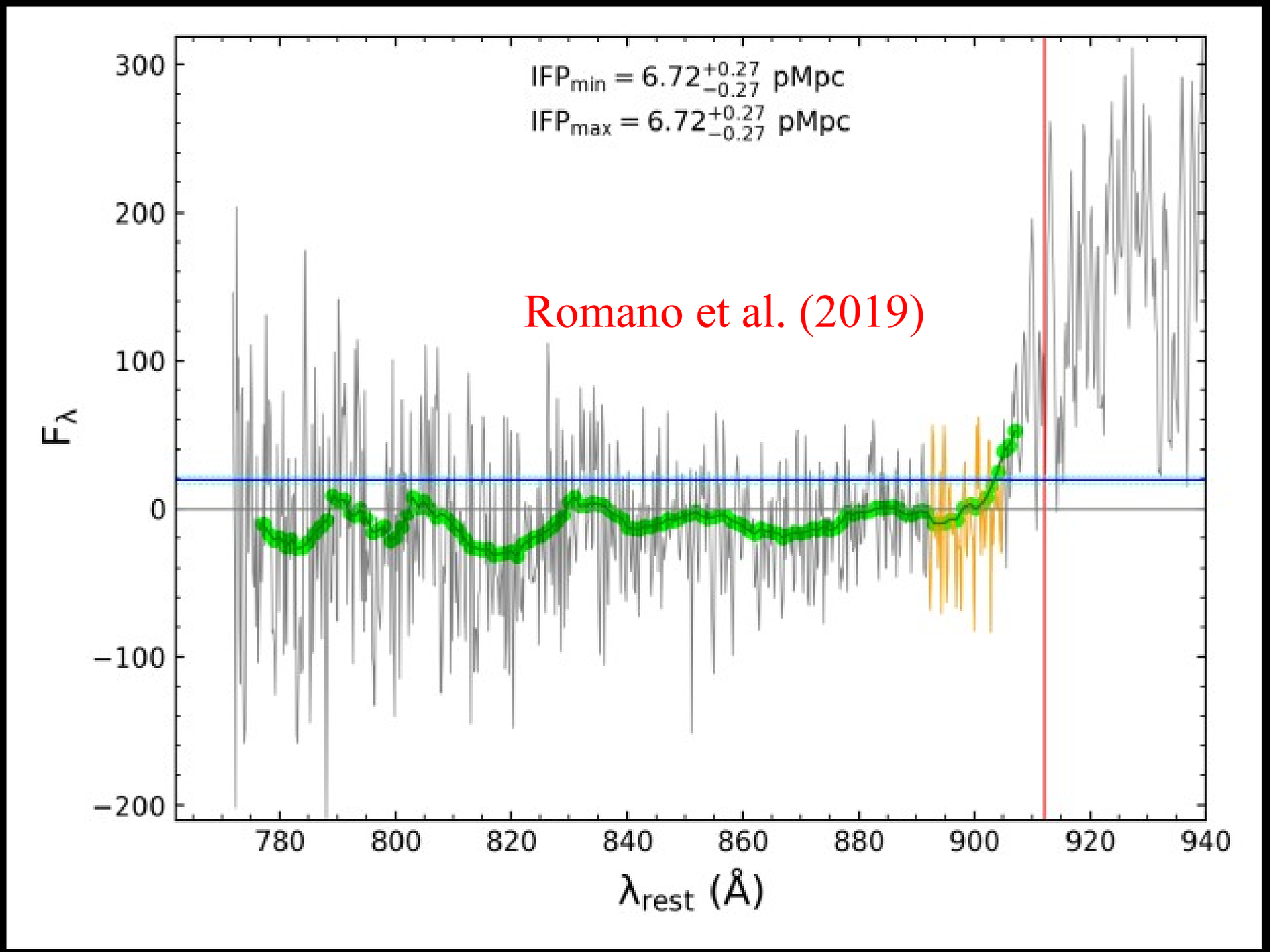

QSOs with short mean free path (MFP) usually show low escape fraction. Associated or intervening absorber ????

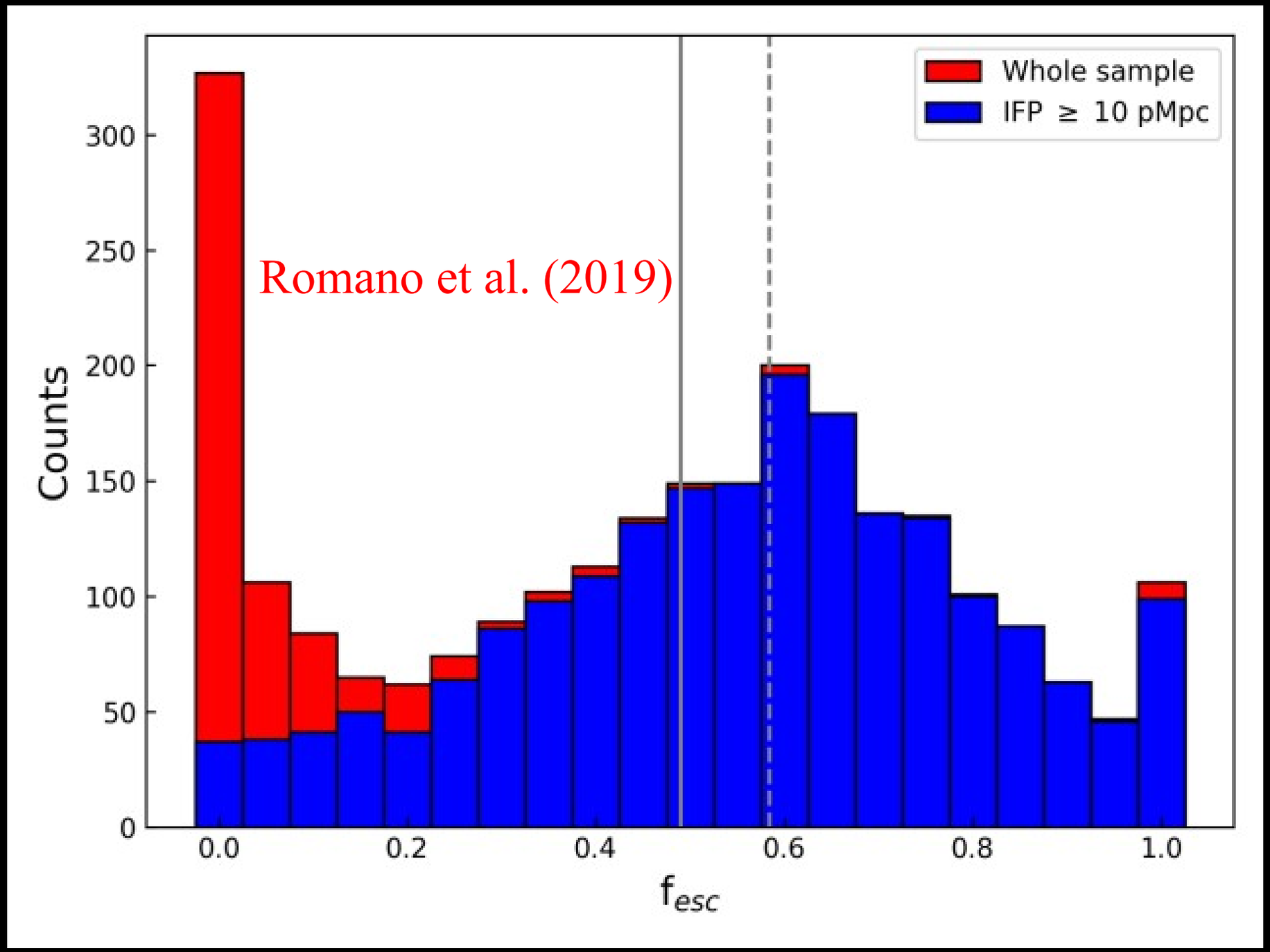
Whole sample
IFP ≥ 10 pMpc
Romano et al. (2019)
Counts
300
250
200
150
100
50
0
0.0
0.2
0.4
0.6
0.8
1.0
f_{esc}

The LyC Escape Fraction of faint AGNs

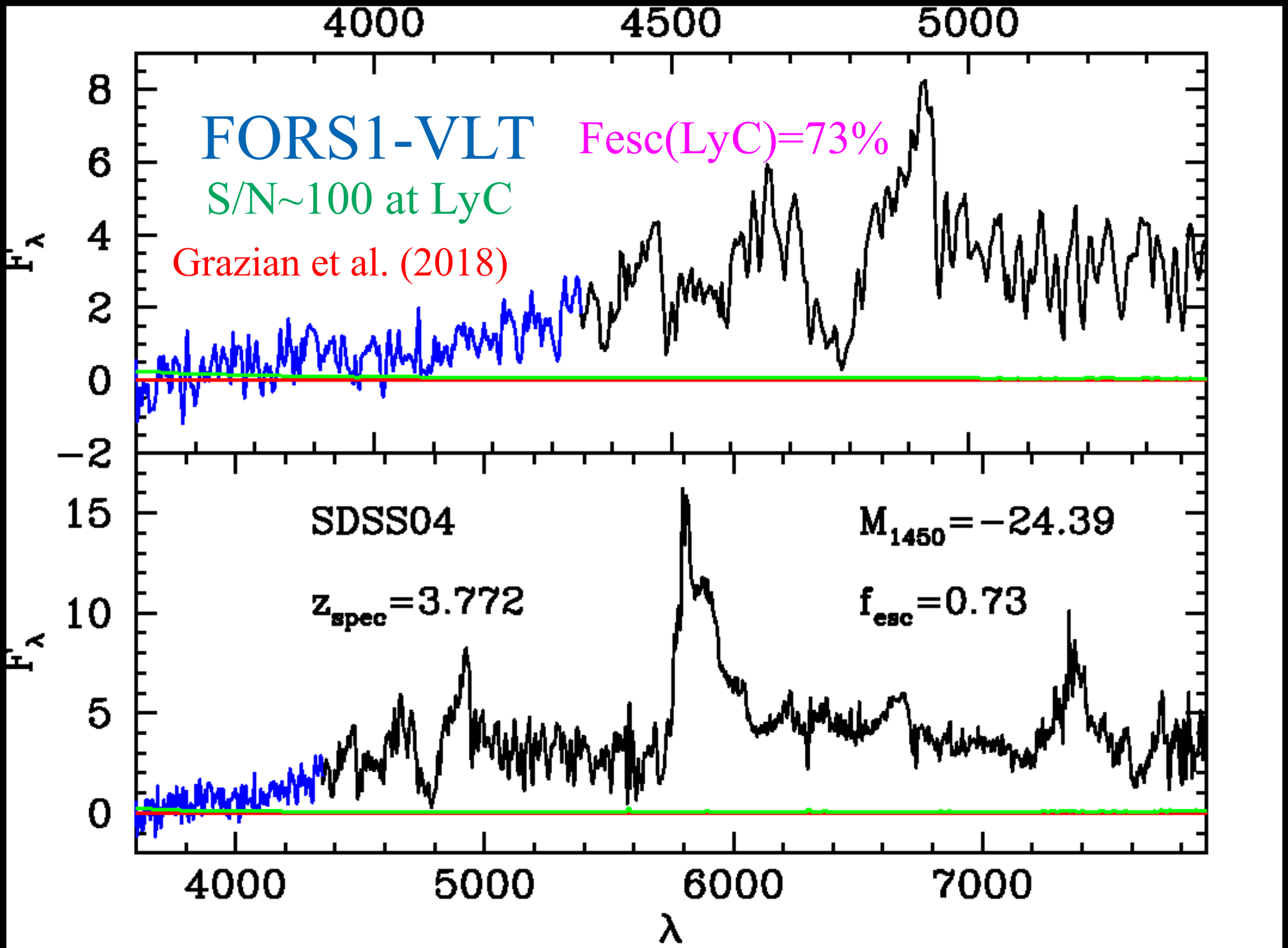

Name	z_{spec}^{new}	$f_{esc}(LyC)$	S/N	M_{1450}
SDSS36	4.047	0.81	87	–25.14
SDSS32	3.964	0.86	33	–25.13
COSMOS775	3.609	0.74	31	–24.14
SDSS37	4.173	1.00	121	–24.94
NDWFSJ05	3.900	0.44	12	–24.03
SDSS04	3.768	0.73	96	–24.39
COSMOS1782	3.748	0.78	72	–23.26
SDSS20	3.899	0.53	58	–24.71
SDSS27	3.604	1.00	42	–24.22
COSMOS955	3.715	0.51	84	–24.65
COSMOS1311	3.736	0.51	29	–24.53
SDSS3777	3.723	0.61	26	–24.62
SDSS3793	3.743	0.84	12	–24.51
SDSS3785	3.769	0.88	20	–24.63
SDSS3832	3.663	0.88	11	–24.72
UDS10275	4.096	0.75	27	–23.80
MEAN	3.82	0.74		–24.46

No evolution of LyC escape fraction with luminosity for z~4 QSOs down to M1450~-23.

We can assume that fesc is constant also at fainter luminosities (M1450=-18).

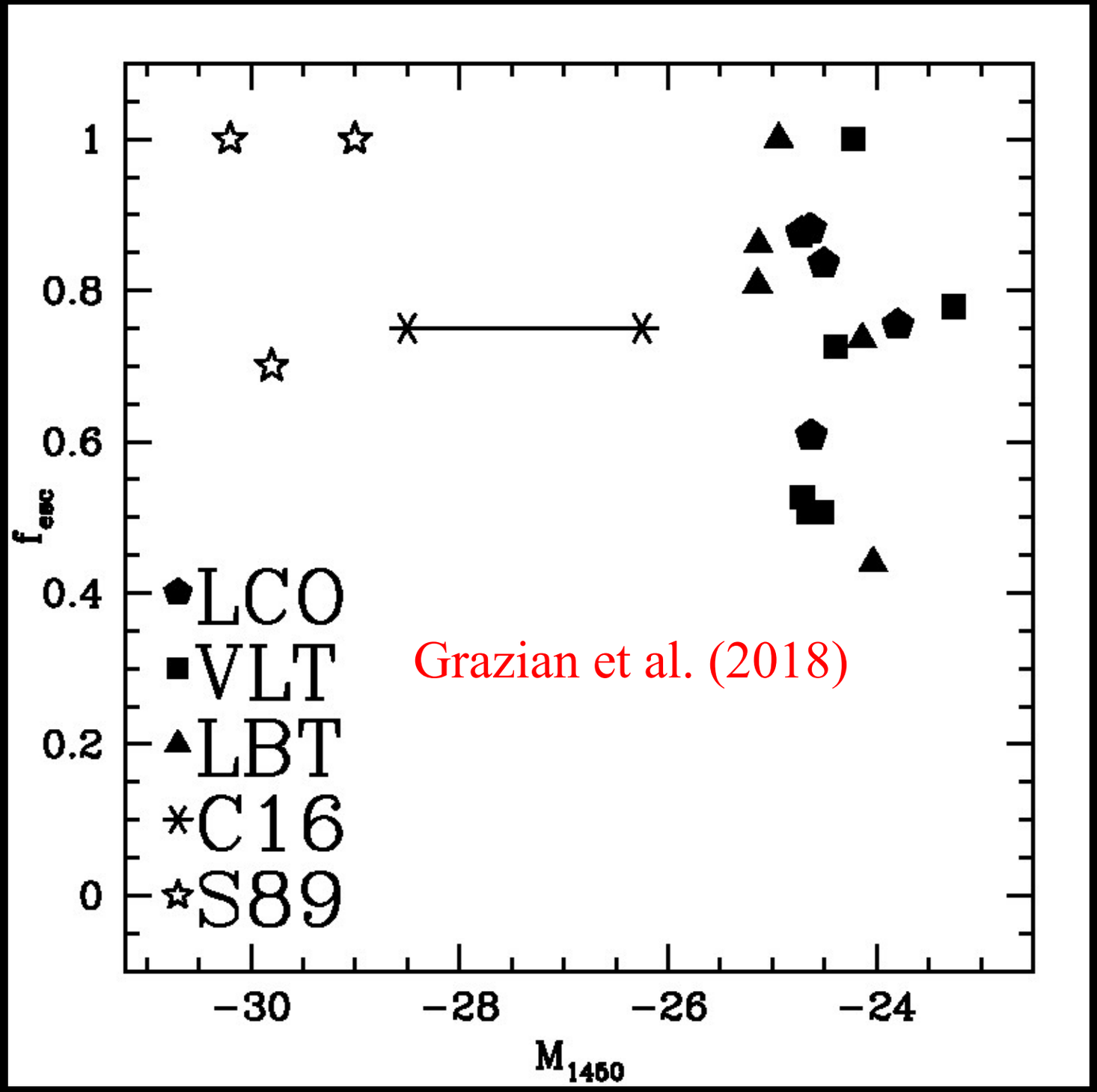

The photo-ionization rate of AGNs

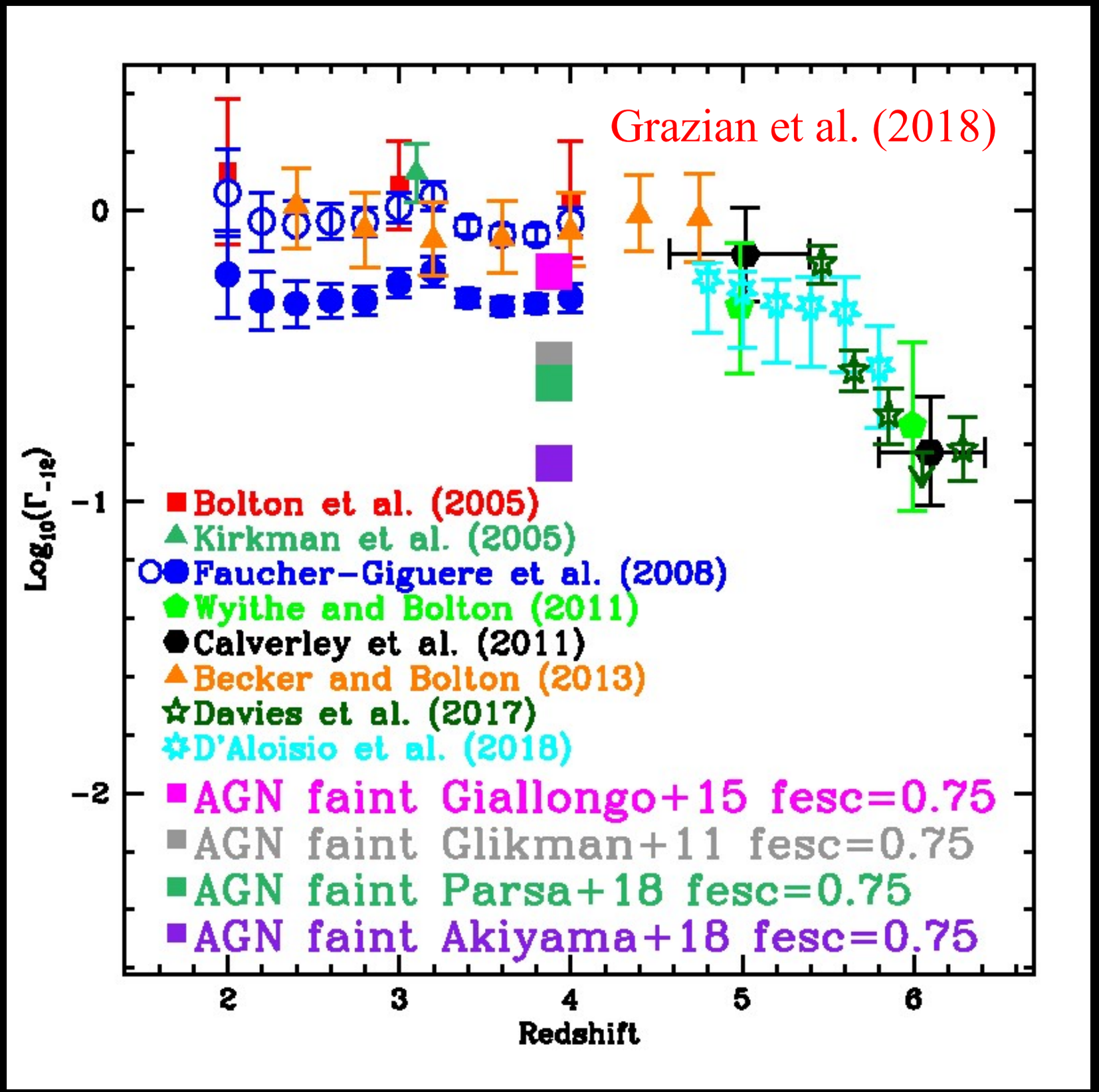

Assuming fesc=75%, QSOs/AGNs can produce 50-100% of ionizing emissivity at z~4 if faint-end Luminosity Function is steep.

Steep QSO LFs have been found by Glikman et al. (2011), Giallongo et al. (2015, 2019), Grazian et al. (2020, 2022), Boutsia et al. (2018, 2021), Harikane et al. (2023).

Summary

LyC escape fraction of bright QSOs and faint AGNs:

1-Spectra should be preferred w.r.t. broad and narrow-band imaging for LyC escape fraction determination.

2-At z<1, bright QSOs and faint AGNs have fesc~100%.

3-At 1<z<4, bright QSOs (M1450=-26) have fesc~75%.

4-Strong LyC escape fraction of faint (M1450<-23) AGNs at z>4 is substantial (~75%). No evolution of LyC escape fraction with Luminosity (Cristiani et al. 2016; Grazian et al. 2018).

5-High space density of bright QSOs and faint AGNs at z~4 (Boutsia et al. 2018, 2021; Giallongo et al. 2015, 2019; Harikane et al. 2023). High space density of bright QSOs at z~5 (Grazian et al. 2022).

At z~4-5 AGNs can produce 50-100% of HI ionizing background.

AGNs could be the main producers of photo-ionizing background at z>4.

Thank you!